A new convective model of the Weddell Polynya

Deep convection in the Southern Ocean

Daan Boot

July 2019

Delft University of Technology

Cover image: Aerial view of the Weddell Polynya. Credit: Jan Lieser, ACE CRC, Australia. Retrieved from: phys.org.

A new convective model of the Weddell Polynya

Deep convection in the Southern Ocean

by

D.B. Boot

to obtain the degree of Master of Science
at the Delft University of Technology,
and Utrecht University
to be defended publicly on Tuesday July 5, 2019 at 11:00 AM.

Student number:	4522451	
Project duration:	October 1, 2018 – July 5, 2019	
Thesis committee:	Dr. C. A. Katsman,	TU Delft (chair)
	Prof. dr. J. D. Pietrzak,	TU Delft
	Prof. dr. ir. H. A. Dijkstra,	Utrecht University
	R. M. Van Westen, MSc	Utrecht University

An electronic version of this thesis is available at `http://repository.tudelft.nl/`.

Preface

Before you lies my thesis about the Weddell Polynya. A thesis for a double degree in Climate Physics at Utrecht University and Hydraulic Engineering at Delft University of Technology. This thesis is the product of 7 years as a student. After a bachelor and two masters, life as an adult really begins.
During the last months I have received help and support of many people. First of all I would like to thank my supervisors, and members of the assessment committee. I would like to thank Henk for the introduction to this topic, and for his guidance throughout the project. I want to thank René for his help, feedback, and his enthusiasm which further increased my own enthusiasm for this research. I would like to thank Caroline and Julie for their feedback on my work.
I would also like to thank my family and friends for their support and help throughout the years. And last, but definitely not least, I would like to thank my girlfriend Latifa. The last year you have given me the love, support, and confidence to finish my studies. Thank you!

Daan Boot
June 2019

Summary

The Weddell Polynya, a large hole in the Antarctic sea ice, reappeared in 2017. Earlier events of the Weddell Polynya have been observed in the 1970's, 1994 and 2016. The polynya forms in the Weddell Sea approximately 800km offshore in the vicinity of an underwater seamount: Maud Rise, around 65°S and 0°E (Fig. 1). The polynya forms due to deep convection in a weakly stratified environment. Several processes have been suggested to induce deep convection, but the relative importance of these processes are not clear. There is a contrast in literature with studies suggesting the polynya is an irregular event governed by surface processes. Studies with (high resolution) climate models suggest a dominant period for the Weddell Polynya related to subsurface heat accumulation. In this study this contrast is looked at by comparing two studies. Martinson et al. (1981) suggest the polynya is an irregular event and caused by brine rejection. van Westen and Dijkstra (2019) suggest that the polynya has a dominant period of 25 years, related to subsurface heat accumulation with the same dominant period. This period is caused by internal ocean dynamics in the Southern Ocean.

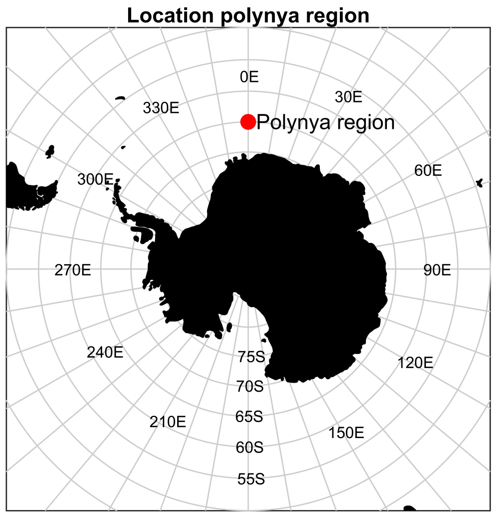

Fig. 1: Location of the polynya region (65°S. 0°E).

To look into the contrast, a simple one-dimensional, vertical, convective model with two layers of constant depth, and uniform characteristics was used, which is based on Martinson et al. (1981). The model simulates the development of temperature, salinity and sea ice thickness. There are four different regimes differentiated on ice cover and static stability. The transitions between the ice covered and ice free regimes are melting and freezing. The transitions between the stable and mixed regimes are overturning and stabilisation. The model is forced at the surface with a freshwater and heat flux. Each layer is forced with a horizontal advective flux. Two different model set ups have been used: (1) The Martinson set up has constant subsurface characteristics and uses no horizontal advective fluxes. This set up is based on Martinson et al. (1981) to reproduce the original results and to test the long term behaviour of the model; (2) the Extended set up uses the complete model. This set up is used to reproduce general features of the results of van Westen and Dijkstra (2019), to look into the importance of the different subsurface fluxes (representing heat and salt accumulation), and to look into the periodicity. The period of the subsurface flux in this set up is 25 years. To test the influence of noise on both set ups, white noise was added to the freshwater flux.

The original results of Martinson et al. (1981) were not produced due to an incomplete parameter documentation. However, the model behaviour of the Martinson set up was the same. The model has two stable solutions. It either has a yearly repeating stable cycle, or it has a yearly repeating cycle with two overturns. With this set up it is not possible to simulate multiple polynya events. Addition of white noise to the freshwater flux only affects the timing of the first overturn.

The general features of the model simulation of van Westen and Dijkstra (2019) are resolved with this simple model. The extended model set up simulates periodic polynya behaviour with the same dominant period as the subsurface fluxes (25 years). van Westen and Dijkstra (2019) suggest that heat accumulation is the dominant driver. This was not confirmed, since cases with no subsurface heat accumulation performed equally well as cases including subsurface heat accumulation. The same dominant period of 25 years for the polynya events was also seen with the addition of white noise.

In this study the importance of surface processes versus subsurface processes for the Weddell Polynya was assessed. Also the periodicity of the polynya was investigated. The conclusions of Martinson et al. (1981) that the polynya is an irregular event caused by brine rejection was tested and compared with possible periodicity caused by subsurface heat accumulation. Results show that the Martinson set up is unable to simulate multiple polynya events, which suggests physical processes are missing. This means irregularity of the polynya does not occur. With the introduction of periodic subsurface forcing, periodic polynya events were simulated, showing the importance of subsurface processes. The results also show that overturning is preceded by a short period of ice growth and thus brine rejection, which suggests brine rejection causes deep convection. However, brine rejection only results in deep convection in a preconditioned ocean, where the stratification is not too strong. The ocean is preconditioned by subsurface heat and salt accumulation. Therefore the deep convection is governed by these subsurface processes. The conclusion of van Westen and Dijkstra (2019) that heat accumulation is dominant has not been confirmed. Other surface related processes as the wind field and eddy shedding at Maud Rise are not unimportant, however, I suggest that this only influences the size, duration and exact location of the polynya, but that the initial formation and periodicity of the polynya is governed by subsurface heat and salt accumulation.

Contents

List of Figures

List of Tables

List of symbols

Abbreviations

Abbreviation	Full name
ACC	Antarctic Circumpolar Current
CESM	Community Earth System Model
GFDL CM2-0	Geophysical Fluid Dynamics Laboratory Coupled Model version 2.0
KCM	Kiel Climate Model
PFB	Periodic Flux Both
PFH	Periodic Flux Heat
PFS	Periodic Flux Salt
POP	Parallel Ocean Program
REF.1	Reference case 1
REF.2	Reference case 2
SAM	Southern Annular Mode
SOM	Southern Ocean Mode
WDW	Warm Deep Water
WP	Weddell Polynya

Latin symbols

Symbol	Unit	Description
C_p	J kg^{-1} °C^{-1}	Specific heat of sea water
E	m s^{-1}	Evaporation
f	m s^{-1}	Freshwater input
f_{NP}	m s^{-1}	Freshwater input during the non-polynya regime
f_P	m s^{-1}	Freshwater input during the polynya regime
F	g/kg m s^{-1}	Freshwater flux
F_{S1}	g/kg s^{-1}	Horizontal advective salt flux in the surface layer
F_{S2}	g/kg s^{-1}	Horizontal advective salt flux in the subsurface layer
F_{T1}	°C s^{-1}	Horizontal advective heat flux in the surface layer
F_{T2}	°C s^{-1}	Horizontal advective heat flux in the subsurface layer
h	m	Depth of layer 1
H	m	Depth of the water column
K	m s^{-1}	Turbulent diffusion coefficient
K_S	m s^{-1}	Coefficient for salt transfer between the two layers

Symbol	Unit	Description
K_T	m s^{-1}	Coefficient for heat transfer between the two layers
L	J kg^{-1}	Latent heat of sea ice
P	m s^{-1}	Precipitation
Q_{ia}	W m^{-2}	Ice-atmosphere heat flux
Q_{oa}	W m^{-2}	Ocean-atmosphere heat flux
S	g/kg	Salinity
S_1	g/kg	Salinity surface layer
S_2	g/kg	Salinity subsurface layer
S_{b1}	g/kg	Background salinity related to the horizontal advective salt flux in the surface layer
S_{b2}	g/kg	Background salinity related to the horizontal advective salt flux in the subsurface layer
T	°C	Temperature
T_1	°C	Temperature of the surface layer
T_2	°C	Temperature of the subsurface layer
T_{b1}	°C	Background temperature related to the horizontal advective heat flux in the surface layer
T_{b2}	°C	Background temperature related to the horizontal advective heat flux in the subsurface layer
T_f	°C	Freezing temperature of sea water

Greek symbols

Symbol	Unit	Description
α	°C^{-1}	Thermal expansion coefficient
β	(g/kg)$^{-1}$	Haline contraction coefficient
δ	m	Sea ice thickness
σ	g/kg	Salinity difference between sea ice and sea water
ρ	kg m^{-3}	Density of sea water
ρ_0	kg m^{-3}	Reference density of sea water
ρ_1	kg m^{-3}	Density of layer 1
ρ_2	kg m^{-3}	Density of layer 2
ρ_i	kg m^{-3}	Density of sea ice
τ	s^{-1}	Relaxation time scale

1 Introduction

The Weddell Polynya (WP), a large hole in the sea ice surrounding Antarctica, reappeared in 2017. During austral winter the WP forms approximately 800km offshore and is, unlike coastal polynyas, completely enclosed by sea ice. Polynyas typically form in the Maud Rise region around 65°S and 0°E (Fig. 2) (Martinson et al., 1981). The first polynyas were observed in the 1970s with newly available satellite images (Carsey, 1980). In 1974, 1975, and 1976 polynyas were present during the entire (!) winter with an areal extent of approximately 2.5×10^5 km^2 (Gordon, Viscbeck and Comiso, 2007). In 2017 the WP reappeared with an approximate area of 0.5×10^5 km^2 (Cheon and Gordon, 2019). Observations also suggest a short-lived polynya in 1994 (Holland, 2001).

After the first observed polynya events in the 1970s several studies have looked into the processes leading to the formation of the WP. The polynyas have a large influence on local surface meteorology. Cloud cover and surface air temperature increase (Moore et al., 2002). The polynyas also influence the ocean. Polynya formation increases the formation of Antarctic Bottom Water (Wang et al., 2017). However, in a changing climate, de Lavergne et al. (2014) suggested that the formation of Antarctic Bottom Water decreases, and more heat is stored in the interior of the ocean, which increases thermosteric sea level rise. de Lavergne et al. (2014) also suggested that the absence of large scale polynyas from the 1970s to 2014, could contribute to contemporary trends in the climate system of the Southern Hemisphere, such as slowed surface warming and sea ice expansion. This suggests that the polynyas not only affect local surface meteorology, but also the climate in the Southern Hemisphere.

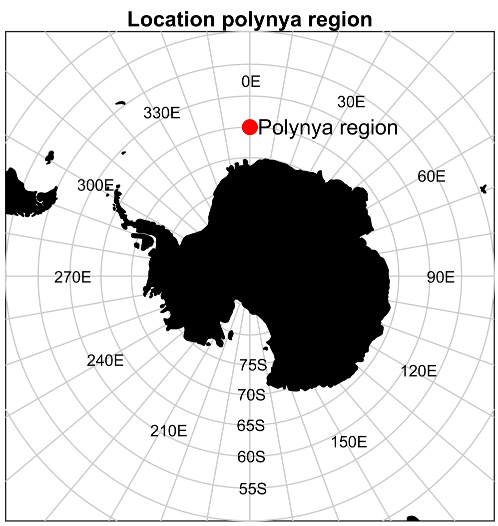

Fig. 2: Location of the polynya region (65°S. 0°E).

To be able to represent polynyas in climate models, a good understanding is necessary. However, there is no clear consensus on the relative importance of the different atmospheric and oceanic processes in this region. It is clear that open ocean convection plays an important role. Martinson et al. (1981) used a simple 1D vertical convective model to show that deep convection is the only process that is able to supply the amount of heat necessary to melt sea ice with the areal extent of the WP. They conclude that deep convection is caused by brine rejection and that the period of deep convection is irregular. They also state that the preconditioning of the ocean in this region is an important factor for deep convection. The stratification in this region needs to be weakened before deep convection can be induced. However, the processes governing this preconditioning of the ocean are what remains less clear, and it is still not completely clear which processes trigger the deep convection in this region. Some studies looked into atmospheric processes: Parkinson (1983) showed that polynya formation is dependent on the wind field, and not only caused by oceanographic processes. With a constant ocean heat flux, she showed that a polynya can form in the middle of a cyclonic wind field. This is the effect of a divergent stress in the ice caused by the wind field. The wind field is also discussed in Francis et al. (2019). They suggested that the origin of the 2017 event is purely dynamical instead of thermodynamical. During austral winter in 2017 there were unusual frequent and intense cyclones present above the polynya region causing ice divergence in this region. However, for the wind field to cause a WP with the area of the 1970's WP, wind speeds above 50 m s^{-1} are necessary (Martinson et al., 1981). Therefore this process is not sufficient to explain all polynya events in this region. Another atmospheric process related to the WP is the Southern Annular Mode (SAM) index. In Gordon et al. (2007) it is suggested that a persisting negative SAM leads to drier than usual conditions in the Southern Ocean. This results in a saltier than usual top layer, and a weaker than usual stratification. The reduced stratification preconditions the ocean, and in combination with a La Niña event (increased sea ice formation, and thus increased brine rejection) deep convection could be induced. The SAM was also related to the size of the WP by Cheon and Gordon (2019). Besides atmospheric processes, dynamical processes have also been mentioned to be responsible for preconditioning the ocean in the polynya region. Holland (2001) used a coupled sea-ice general circulation model with an idealised seamount to show the effect of eddy shedding at the flanks of Maud Rise on the sea ice. He suggests that the flow impinging on Maud Rise gains cyclonic vorticity at the northeastern flank due to vortex stretching. This would result in a divergent stress on the sea ice, which opens the ice pack. In this opening, atmospheric, thermodynamical feedbacks cool the surface layer, making it denser, which could result in deep convection. Another topographically induced effect are Taylor cap dynamics. A Taylor cap is a dome of water above a seamount with almost no interactions with its surroundings. It is suggested this weakens the stratification above the seamount (Alverson and Owens, 1996; Kurtakoti et al., 2018), making it more vulnerable for static instability. Through these dynamical effects, Maud Rise also influences the sea ice. This effect is visible in observations of a halo of low ice concentrations over the flanks of Maud Rise (Lindsay et al., 2004). The different atmospheric and dynamical processes all have an impact on polynyas. What these processes have in common, is that they focus on densification of the surface layer. Furthermore, these processes do not show a dominant period for the WP.

This is in contrast with results from climate models. Climate models give us the opportunity to study deep convection and WP events in the Southern Ocean. Studies using such climate models show a multidecadal to a multicentennial periodicity for the WP (Martin, Park and Latif, 2013; Zanowski, Hallberg and Sarmiento, 2015; Latif, Martin, Reintges and Park, 2017; Weijer et al., 2017). Several climate models show build up of heat in the subsurface layer. Examples are the Kiel Climate Model (KCM) (Martin et al., 2013), the Community Earth System Model (CESM) (van Westen and Dijkstra, 2019) and the GFDL CM2-0 Model (Dufour et al., 2017). The build up of heat is essential for polynya formation. Through buoyancy gain of the subsurface layer, deep convection is induced, which results in polynya formation (Martin et al., 2013; Latif et al., 2017; Reintges et al., 2017). Stratification is shown to be important in the model studies of Latif et al. (2017) and Reintges et al. (2017): they state that in the KCM a stronger stratification results in a longer period for the WP, because more buoyancy gain is necessary to overcome the more stable stratification. In addition, Weijer et al. (2017) showed the importance of the resolution of the climate model. In their high resolution run (0.1°) polynyas were observed, whereas in the low resolution run (1°) no polynyas were simulated. This is confirmed by Dufour et al. (2017) using the GFDL CM2-0 model with a nominal ocean grid spacing of 0.25 ° and 0.1°. In their study they show the occurrence of deep convection itself is not sufficient to create polynyas. If the subsurface heat reservoir cannot supply enough heat to melt all the sea ice, an opening, and thus a polynya will not form. Therefore it is important that the stratification is strong enough to allow for the build up of heat. The strength of this stratification is related to the resolution of the models, in both the horizontal grid and the bathymetry. This is related to the ability of a model to represent restratifying, mesoscale eddies. The restratifying effect of the mesoscale eddies results in more heat build up in the subsurface layer. Therefore higher resolution models allow for more heat accumulation which is shown to be important for polynya formation. These higher resolution models also approach the observed periodicity of the WP (20 or 40, if not counting the 1994 event, years) better than low resolution models. These studies show the importance of subsurface processes for the Weddell Polynya, and moreover, they also show a dominant periodicity.

From these climate model studies two conclusions can be drawn: both resolution and heat accumulation are important factors for representing polynyas. Another model study by van Westen and Dijkstra (2019) suggested that the WP is part of an intrinsic variability of the climate system and that the deep convection related to the WP is mainly caused by subsurface heat transport. van Westen and Dijkstra (2019) relate the accumulation of heat in the subsurface layer to the the Southern Ocean Mode (SOM), a multidecadal mode of intrinsic variability of sea surface temperature in the Southern Ocean caused by eddy-mean flow interactions (Jüling et al., 2018). The SOM was identified by Le Bars et al. (2016) in an eddying version of the Parallel Ocean Program (POP). In Le Bars et al. (2016) and in a CESM simulation of van Westen and Dijkstra (2017) the SOM was identified with a 40 year period. van Westen and Dijkstra (2019) used an extended run of the same model simulation as van Westen and Dijkstra (2017) in which the period reduced to 25 years due to further adjustment of the model. In this simulation, a correlation was found between the SOM and the presence of the WP. van Westen and Dijkstra (2019) suggested that heat content anomalies propagate from the SOM region (50°S - 35°S, 50°W - 0°W) via the Antarctic Circumpolar Current (ACC) to 30°E where they enter the Weddell Gyre as Warm Deep Water (WDW). The anomalies propagate to the polynya area near Maud Rise where they cause heat accumulation in the subsurface layer. The lag between a positive SOM phase and a polynya event is on the same order as the time necessary to propagate from the SOM region to the polynya region with the ambient current (10 years). The SOM is able to explain the subsurface heat accumulation near Maud Rise. The importance of this subsurface heat accumulation in the study of van Westen and Dijkstra (2019) contrasts studies which focus on surface processes.

This contrast is the result of the lack of consensus on the importance of the different processes. Even though many studies investigated the origin of the WP, there is no consensus on the exact processes leading to the formation and neither on the periodicity of the WP. Several studies have focused on surface processes without a clear dominant periodicity (e.g. Martinson et al., 1981; Holland, 2001; Gordon et al., 2007), while studies with (high resolution) climate models show the importance of subsurface processes with a dominant multidecadal frequency. Though all processes can be important for the size, location and duration of the WP, it is not clear what the most dominant process for the initial formation, and the periodicity of the WP is. In a study of Martinson et al. (1981) the WP was marked as an irregular occurring event caused by brine rejection in a preconditioned ocean. The high resolution CESM simulation of van Westen and Dijkstra (2019) shows a periodic return of the WP due to periodic heat accumulation in the subsurface layer. The contrast between the simple model of Martinson et al. (1981) and the high resolution simulation of van Westen and Dijkstra (2019) is a reason to revisit the original model of Martinson et al. (1981) and to use this model to look into two issues: what is the importance of subsurface forcing relative to surface forcing, and what governs the periodicity of the WP? To look into these issues, first an attempt is made to reproduce the results of Martinson et al. (1981). This model was used to investigate the 1970s polynya. We will test whether multiple events (e.g. the 1970s and 2017 event) can be explained using this model. Secondly, the original model is extended with a dynamical subsurface layer instead of a constant subsurface layer, since observations (Fahrbach et al., 2011), and several climate models (Martin et al., 2013; Latif et al., 2017; Reintges et al., 2017; Kurtakoti et al., 2018; van Westen and Dijkstra, 2019) show an accumulation of heat (and salt) prior to a WP event. Heat and salt fluxes are used to force the subsurface layer. This extended version of the Martinson model is described in Section 2. Two model set ups, and five cases are used to do tests with the model. The results of the different cases are discussed in Section 3. In Section 4 a summary and discussion of the results is given.

2 Model description and experimental set up

The model used in this study is an extended version of the 1D model used in Martinson et al. (1981). The model is extended with an active subsurface layer, and horizontal advective fluxes in both the surface and the subsurface layer. First the model is described (Section 2.1), after which the experimental set up and parameter values are discussed (Section 2.2).

2.1 Model description

The used model is a simple one-dimensional, vertical model with two layers of constant depth and uniform temperature, salinity and density.The model simulates the development of temperature (T), salinity (S), and sea ice thickness (δ) under surface and subsurface forcing. The model has four different regimes, which are differentiated on ice cover (ice free versus ice covered) and static stability (stable, two layered versus unstable, mixed). There are the ice free regimes 1 and 2, and the ice covered regimes 3 and 4. Regimes 2 and 4 are stable ($\rho_1 < \rho_2$), and regimes 1 and 3 are mixed with one uniform layer over the entire depth (Fig. 3).

The model transits through these four regimes. The different regime transitions are displayed with arrows in Fig. 3. There are four different regime transitions: (1) from ice covered regimes to ice free regimes due to complete melt of the sea ice ($\delta = 0$) (regime 4 to

2 and regime 3 to 1); (2) from ice free regimes to ice covered regimes, because the surface layer reaches freezing temperature and sea ice starts to form ($T_1 = T_f$) (regime 2 to 4, and regime 1 to 3); (3) from stable, two layered regimes to unstable, mixed regimes, because the density of the surface layer is equal to or larger than the density of the subsurface layer ($\rho_1 \geq \rho_2$) (regime 2 to 1, and regime 4 to 3). The water column becomes unstable and mixes through overturning; (4) from unstable, mixed regimes to stable, two layered regimes, because of stabilisation of the water column due to a decreasing density of the mixed layer ($-\alpha \frac{dT}{dt} + \beta \frac{dS}{dt} < 0$) (regime 1 to 2, and regime 3 to 4). The mathematical representation of the regime transitions are displayed in Appendix A. It should be noted that for the model to switch between regimes 1 (mixed, ice free) and 3 (mixed, ice covered) the entire water column should reach freezing temperature, which is physically not realistic. This condition is therefore never met.

The model is forced at the surface by a freshwater flux ($F = (P - E) \times 35$ g/kg), and a monthly varying heat flux (Q_{ia} for ice covered regimes and Q_{oa} for open ocean regimes). Both the surface and subsurface layer are subject to a horizontal advective heat and salt flux (F_{T1} and F_{S1} for the surface layer, and F_{T2} and F_{S2} for the subsurface layer) which depend on a background value (T_{b1} and S_{b1} for the surface layer, and T_{b2} and S_{b2} for the subsurface layer) and a relaxation timescale (τ).

Between the two layers, heat and salt transfer is modelled using exchange coefficients (K_T and K_S) which account for upwelling, turbulent exchange and diffusion. In ice covered regimes there is a heat flux present between the sea ice and the underlying layer. This flux is modelled using a turbulent exchange coefficient (K). During ice growth, brine is rejected, and during ice melt, fresh water is added to the surface layer. Brine rejection and melt are modelled using a constant representing the salinity difference between sea ice and seawater (σ), and the rate of ice growth ($\frac{d\delta}{dt}$).

For each regime there is a set of equations determining the temperature and salinity per layer, and the sea ice thickness which represent these processes (Equations 1 to 4). The density per layer is determined with a simple linear equation of state (Equation 5). This equation neglects nonlinear and pressure dependent terms. The differences between the linear equation and versions including the nonlinear and pressure dependent terms are negligible for this study, because the density difference is only determined at the interface between the layers in a highly idealised model (Martinson et al., 1981).

Equations 1 to 4 represent the differential equations resolved in each of the regimes. Equation 1 represents regime 1, Equation 2 regime 2, Equation 3 regime 3, and Equation

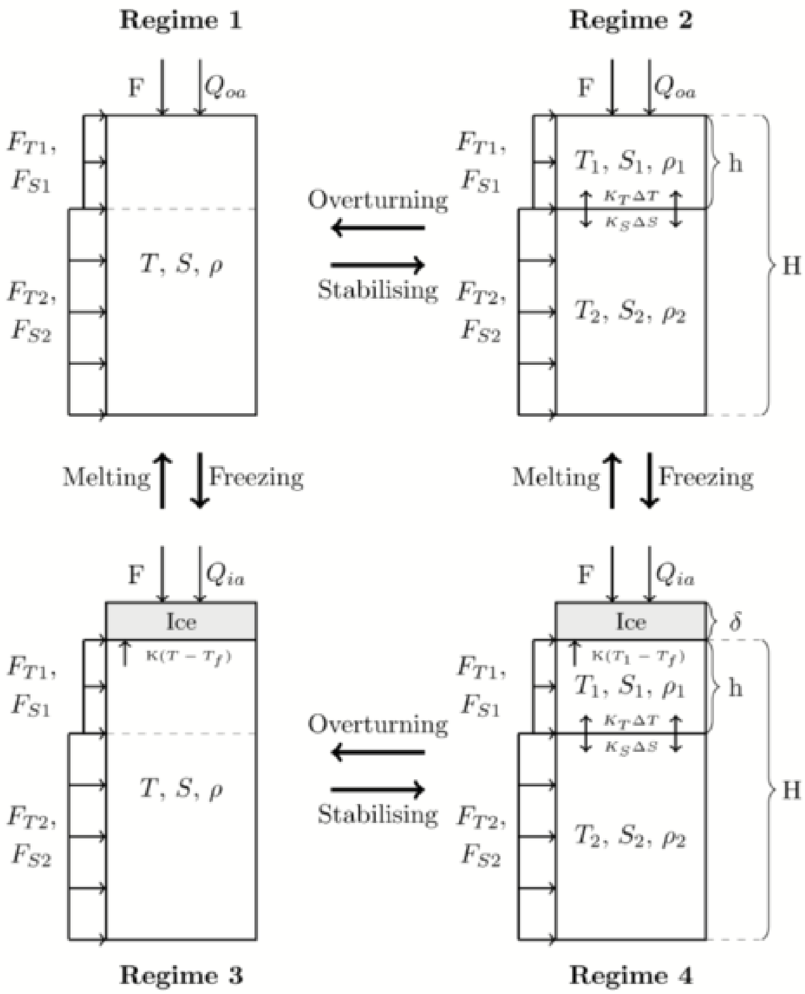

Fig. 3: A schematic representation of the different regimes of the model. This model is an extension of the model used in Martinson et al. (1981). The parameters displayed in the figure are explained in the text. The directions and size of the arrows are not necessarily a representation of the actual direction and magnitude of the fluxes. The actual size and direction are dependent on the state of the model. Positive fluxes represent fluxes entering the system. Regime transitions are shown by bold arrows.

4 represents regime 4. Regime 1:

$$H\frac{dT}{dt} = \frac{Q_{oa}}{\rho_0 C_p} + \tau(T_{b1} - T)h + \tau(T_{b2} - T)(H - h) \tag{1a}$$

$$H\frac{dS}{dt} = -F + \tau(S_{b1} - S)h + \tau(S_{b2} - S)(H - h) \tag{1b}$$

$$\delta = 0 \tag{1c}$$

Regime 2:

$$h\frac{dT_1}{dt} = \frac{Q_{oa}}{\rho_0 C_p} + K_T(T_2 - T_1) + \tau(T_{b1} - T_1)h \tag{2a}$$

$$h\frac{dS_1}{dt} = K_S(S_2 - S_1) - F + \tau(S_{b1} - S_1)h \tag{2b}$$

$$\delta = 0 \tag{2c}$$

$$\frac{dT_2}{dt} = \tau(T_{b2} - T_2) + \frac{K_T(T_1 - T_2)}{H - h} \tag{2d}$$

$$\frac{dS_2}{dt} = \tau(S_{b2} - S_2) + \frac{K_S(S_1 - S_2)}{H - h} \tag{2e}$$

Regime 3:

$$H\frac{dT}{dt} = K(T - T_f) + \tau(T_{b1} - T)h + \tau(T_{b2} - T)(H - h) \tag{3a}$$

$$H\frac{dS}{dt} = \sigma\frac{d\delta}{dt} - F + \tau(S_{b1} - S)h + \tau(S_{b2} - S)(H - h) \tag{3b}$$

$$\frac{d\delta}{dt} = \frac{1}{\rho_i L}(-Q_{ia} - \rho_0 C_p K(T - T_f)) + \frac{F}{\sigma} \tag{3c}$$

Regime 4:

$$h\frac{dT_1}{dt} = K_T(T_2 - T_1) - K(T_1 - T_f) + \tau(T_{b1} - T_1)h \tag{4a}$$

$$h\frac{dS_1}{dt} = \sigma\frac{d\delta}{dt} - F + \tau(S_{b1} - S_1)h \tag{4b}$$

$$\frac{d\delta}{dt} = \frac{1}{\rho_i L}(-Q_{ia} - \rho_0 C_p K(T_1 - T_f)) + \frac{F}{\sigma} \tag{4c}$$

$$\frac{dT_2}{dt} = \tau(T_{b2} - T_2) + \frac{K_T(T_1 - T_2)}{H - h} \tag{4d}$$

$$\frac{dS_2}{dt} = \tau(S_{b2} - S_2) + \frac{K_S(S_1 - S_2)}{H - h} \tag{4e}$$

Equation of state:

$$\frac{\rho - \rho_0}{\rho_0} = -\alpha T + \beta S \tag{5}$$

In these equations C_p is the specific heat of seawater with density ρ_0. Ice has a density of ρ_i and latent heat L. The depth of the entire column is H, with a smaller top layer with depth h. α and β are constants in the equation of state representing thermal expansion and haline contraction, respectively. The values of all parameters used in the model are discussed in Section 2.2.

The set of differential equations (Equations 1 to 4) is solved using the ODE15s solver incorporated in Matlab. The ODE15s solver is a variable-step, variable-order solver based on an algorithm by Klopfenstein (1971) using numerical differentiation formulas (NDFs) orders 1 to 5. Tolerances for the absolute and relative error are used to increase the accuracy of the model. These tolerances are set to 10^{-10} and 10^{-8}, respectively. The absolute error tolerance measures when the solution becomes unimportant. The relative error tolerance is the size of the allowable error relative to the magnitude of the solution.

2.2 Experimental set up

The model described in Section 2.1 is used with two different set ups: the 'Martinson' set up and the 'Extended' set up. The 'Extended' set up uses all model components, while in the 'Martinson' set up several components are switched off. The differences between the two set ups, are displayed in Table. 1. The 'Martinson' set up has two different cases (REF.1 and REF.2). The 'Subsurface' set up has three (PFB, PFH, and PFS).

The 'Martinson' set up uses the original model of Martinson et al. (1981). The horizontal advective fluxes (F_{T1}, F_{S1}, F_{T2} and F_{S2}) are switched off, and the subsurface layer is set on a constant value. Two different cases (REF.1 and REF.2) are used which use a different value for K_S. A higher value of K_S results in more salt transfer from the subsurface layer to the surface layer, increasing the density of the surface layer, making it more prone to overturning. Two cases are used because of the completely different behaviour of the cases. REF.1 uses a lower K_S and REF.2 a higher K_S. This means that REF.2 is more prone to show deep convection. With this set up, an attempt is made to reproduce the original results of Martinson et al. (1981). Compared to Martinson et al. (1981) longer runs are used to investigate the long term behaviour of the model.

The 'Extended' set up uses a dynamic subsurface layer and horizontal advective fluxes as described in Section 2.1. The three cases are differentiated on the inclusion of the different components of the subsurface forcing. Case PFB (Periodic Flux Both) uses both a subsurface heat and salt flux. Case PFH (Periodic Flux Heat) uses only a subsurface heat flux. The background value for the subsurface salt flux is set constant at the mean of the periodic subsurface salt flux used in PFH. Case PFS (Periodic Flux Salt) uses only a salt flux, and the background value for the heat flux is set constant at the mean of the periodic subsurface heat flux used in PFH. The aim of this set up is to reproduce the general features of the CESM simulation of van Westen and Dijkstra (2019), where the observed periodicity of the WP events is one of the key features. The different cases are used to assess the importance of the different components of the subsurface forcing.

Cases REF.1 and PFB have also been tested with white noise added to the freshwater flux (F). The aim of these tests was to investigate the influence of noise on the regularity of polynya events. For case PFB the main question was whether the same dominant frequency

Table. 1: The inclusion of different model components, and values for the diffusivity parameters for heat (K_T) and salt (K_S) transfer between the two layers per case. A model component can either be included ('on'), or excluded ('off'). The model component 'dynamic T_2 and S_2' stands for an active subsurface layer. If this component is excluded, the set up uses a constant subsurface layer. If either F_{T2} or F_{S2} is excluded, the background value corresponding to the flux is set constant. The model components containing 'F' represent fluxes with subscripts representing the horizontal heat (T) and salt (S) fluxes in either the surface (1), or subsurface (2) layer.

Model component	Dynamic T_2 and S_2	F_{T1}, F_{S1}	F_{T2}	F_{S2}	K_T [10^{-6}m s^{-1}]	K_S [10^{-6}m s^{-1}]
Martinson model set-up						
REF.1	off	off	off	off	5.00	1.375
REF.2	off	off	off	off	5.00	2.00
Extended model set-up						
PFB	on	on	on	on	2.82	2.82
PFH	on	on	on	off	2.80	2.80
PFS	on	on	off	on	2.80	2.80

was still visible. For REF.1 the effect of noise on inducing deep convection wass assessed.

Parameter values per case are displayed in Table. 2. The parameter values are either taken from Martinson et al. (1981), based on the CESM simulation of van Westen and Dijkstra (2019), or they are determined through tuning of the model. If the model is not tuned correctly, the stratification is either too strong and no overturns occur, or the stratification is too weak and the water column overturns each year. The aim of the model is to investigate multiple polynya events, therefore it is necessary to tune the stratification within the model to be able to simulate multiple events. This is done by tuning the heat and salt fluxes between the two layers and between the sea ice and the surface layer. The forcing of the model (the horizontal fluxes, surface heat fluxes, and freshwater flux), is displayed in Section 3. The forcing and certain parameter values, as described in the next part, differ from the original study of Martinson et al. (1981). These differences are expected to change the exact results of the model, but not the general model behaviour.

The typical depth of the layers has been determined from the CESM simulation of van Westen and Dijkstra (2019). The depth of the surface layer (h) is set to 160m, because in CESM potential density data shows a clear homogeneous layer below 160m (Fig. 14 in Appendix B). This compares well to the value used in Kurtakoti et al. (2018) (150m), but is smaller than the value used in Martinson et al. (1981) (200m). The depth of the entire layer (H) is set on 2000m. This is the approximate mixed layer depth during convective events in the CESM simulation (Fig. 15 in Appendix B). This magnitude corresponds well to values presented in Fahrbach et al. (2011) for the lower limit of where WDW is found, and in Dufour et al. (2017) for the depth of the subsurface layer. It is however half the size

Table. 2: Parameter values for constants. Superscripts show whether the parameter value is determined from the CESM simulation of van Westen and Dijkstra (2019) (C), determined through tuning (t), or taken from Martinson et al. (1981) (M). The initial conditions are chosen.

Parameter	Value	Parameter	Value	Parameter	Value
h^C [m]	160	$\delta(0)$ [m]	1	C_P^M [J kg^{-1} °C^{-1}]	4.18×10^3
H^C [m]	200	α^M [°C^{-1}]	5.82×10^{-5}	L^M [J kg^{-1}]	2.5×10^5
K^t [m s^{-1}]	10^{-4}	β^M [(g/kg)$^{-1}$]	8×10^{-4}	σ^M [g/kg]	30
$T_1(0)$ [°C]	0.1	ρ_0^M [kg m^{-3}]	1000	T_f^M [°C]	-1.86
$S_1(0)$ [g/kg]	34.2	ρ_i^M [kg m^{-3}]	900		

of the value used in Martinson et al. (1981) (4000m).

The turbulent exchange coefficient K, and the exchange coefficients K_T and K_S have been used as tuning parameters for the different cases. K was set to 1×10^{-4} ms^{-1} for all cases (in Martinson et al. (1981) this value was 3×10^{-4} ms^{-1}). For the Martinson set up, double diffusive processes are important, since K_T and K_S have different values. For the subsurface set up double diffusion is not taken into account. The values per case are shown in Table. 1. To compare the magnitude of these parameters with values used in literature the values need to be converted from ms^{-1} to m^{2}s^{-1}, which is the usual unit for vertical diffusivity parameters. This is done by multiplying these values with the depth of the surface layer (i.e. 160m). This results in values between 2.2×10^{-4} m^{2}s^{-1} and 8×10^{-4} m^{2}s^{-1}. Comparable values are found in a model study of Dufour et al. (2017) for this same location and in observations from Shaw and Stanton (2014). The values used in this study are larger than the values used in Martinson et al. (1981) ($K_T = 7 \times 10^{-7}$ ms^{-1} and $K_S = 10^{-7}$ ms^{-1}).

The adjustment time of the model to the initial conditions is a few years. The long term behaviour of the model is not sensitive to the exact initial conditions when two constraints on the initial are taken into account. Firstly, the starting regime of the model should be taken into account. If the model starts in stable regimes 2 and 4, the density of the surface layer should be lower than that of the subsurface layer. Also the ice cover should be taken into account. Ice free regimes 1 and 2 should be initiated without sea ice ($\delta = 0$), and ice covered regimes 3 and 4 should be initiated with sea ice ($\delta > 0$). And secondly, the adjustment time during the first years need to be taken into account. This adjustment time is approximately 2 years for T_1 and δ. Overturning during this adjustment time due the initial conditions is undesirable. Therefore the stratification of the initial conditions should be strong enough to prevent overturning in the adjustment time. In this study these two constraints have been taken into account to ensure no overturning occurs in the adjustment period. All runs are started on the 1st of January in stable regime 4.

3 Results

In this section the results are displayed. In Section 3.1, the used forcing, determined from the CESM simulation used in van Westen and Dijkstra (2019), is discussed. Secondly, in Section 3.2 an analysis of the model behaviour is given after which the 'Martinson' set up (cases REF.1 and REF.2) is discussed (Section 3.3). The results of the 'Extended' set up (cases PFB, PFH, and PFS) are shown in Section 3.4. And lastly, noise is added to the freshwater flux for cases REF.1 and PFB in Section 3.5.

3.1 Forcing

All cases are forced by the same monthly varying heat flux (Q_{oa} or Q_{ia}) and freshwater flux (F) at the surface. The Extended model set up cases are also forced by horizontal heat and salt fluxes in both layers (FT_1, FS_1, FT_2 and FS_2). The forcing is determined from the CESM simulation used in van Westen and Dijkstra (2019). They determined a region with a probability density function where polynyas were most likely to form in there simulation (2°E - 11°E $\times$ 63.5°S - 66.5°S). The CESM output used for this analysis represents this region and consists of monthly values.

For the ice free regimes (1 and 2) the model is forced by an ocean-atmosphere heat flux (Q_{oa}). In the ice covered regimes (3 and 4), the ice-atmosphere heat flux (Q_{ia}) is used. In the CESM simulation the distinction between ice free and ice covered periods are less clear. In the model used in this study the ice fraction is either 0 or 1, while in CESM the ice fraction ranges between 0 and 1. This ice fraction influences the heat fluxes in the CESM simulation. When the ice fraction in the polynya region drops below 0.5, a large increase in the surface heat flux is observed. Therefore, if the ice fraction in the CESM simulation in this area is smaller than 0.5, the heat flux is considered to represent a ice free regime in the model used in this study (Q_{oa}). When the ice fraction in CESM is larger, the heat flux is considered to represent ice covered regimes (Q_{ia}). In months without sea ice, the ice-atmosphere flux is set equal to the ocean-atmosphere heat flux. This results in the monthly heat fluxes displayed in Table. 3. These monthly values are interpolated linearly in the model as shown in Fig. 16 in Appendix B.

The presence of a polynya changes the magnitude of the freshwater flux (F) as it results in more evaporation. Therefore the model uses a different freshwater flux during a polynya period relative to a non-polynya period. The values for the non-polynya regime freshwater input (f_{NP}), and the polynya regime freshwater input (f_P), determined from the CESM simulation, are presented in Table. 3. These monthly values are interpolated linearly in the model s shown in Fig. 17 in Appendix B. The total freshwater input (f) is 0.38 m year^{-1}

Table. 3: Ocean-atmosphere heat flux (Q_{oa}) in Wm^{-2}, ice-atmosphere heat flux (Q_{ia}) in Wm^{-2}, and the freshwater input (*f=P-E*) in mm/day for polynya (P) and non-polynya (NP) regimes per month determined from the CESM simulation of van Westen and Dijkstra (2019). Positive values represent fluxes going into the ocean or the sea ice (warming and net precipitation). Negative values represent fluxes going to the atmosphere (cooling and net evaporation).

Month	Q_{oa}[Wm^{-2}]	Q_{ia}[Wm^{-2}]	f_P[mm/day]	f_{NP}[mm/day]
Jan	61.4	61.4	0.91	0.87
Feb	-23.6	-23.6	1.17	1.06
Mar	-90.8	-90.8	0.96	1.04
Apr	-144.1	-86.1	0.62	0.86
May	-161.3	-90.3	0.96	0.93
Jun	-202.3	-79.3	0.47	1.17
Jul	-246.9	-72.5	0.22	1.09
Aug	-205.6	-65.2	0.13	1.07
Sep	-76.9	-40.3	0.62	1.27
Oct	-43.0	-1.2	0.69	1.32
Nov	107.4	44.1	0.78	1.11
Dec	128.2	128.2	0.44	0.79

for non-polynya years, and 0.24 m year^{-1} for polynya years. The first value is within the range presented in Martinson et al. (1981) (0.38-1.73 m year^{-1}). This range is based on estimates which are based on limited observations. The value for polynya years is out of this range. However, this range is based on observations, and in 1981 no observations were available for the freshwater input during a polynya event.

For the four horizontal advective fluxes (FT_1, FS_1, FT_2 and FS_2) a background temperature (T_{b1} and T_{b2}) and salinity (S_{b1} and S_{b2}) are used. All four values were determined from the CESM simulation. The first layer uses a constant background temperature ($T_{b1} = -0.33$°C). The constant background salinity (S_{b1}) for the surface layer was slightly changed to tune the model, to be able to simulate multiple polynya events. The determined value of 34.5 g/kg was changed to 34.4814 g/kg. The background temperature and salinity of the subsurface layer (T_{b2} and S_{b2}) are periodic in nature and are shown in Fig. 4. CESM model years 210-235 were used, and the temperature and salinity are averaged over the layer between 200m and 1000m. In this layer most of the heat and salt accumulation is seen in van Westen and Dijkstra (2019).

For all horizontal fluxes a relaxation timescale (τ) is used. This parameter is based on the advective time scale of the Weddell Gyre ($\tau_A = \frac{L}{U}$). The typical velocity scale in the Weddell Gyre is on the order of 5×10^{-2}m s^{-1} (Klatt et al., 2005), and the typical length scale of the Weddell Gyre is 10^6m. This results in an advective time scale of 230 days. To be able to represent multiple events, τ is set on $\frac{1}{200\ days}$.

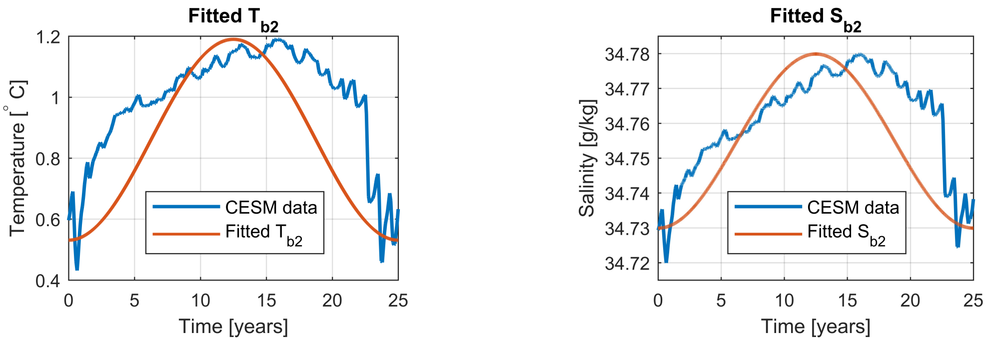

(a) T_{b2} fitted to CESM data.

(b) T_{s2} fitted to CESM data.

Fig. 4: (a) Subsurface background temperature (T_{b2}) (red line) used in the extended model set up fitted to the CESM simulation of van Westen and Dijkstra (2019) (blue line). A sinusoidal function is fitted to CESM model years 210-235. The CESM simulation data (blue line) is averaged over depth (200-1000m). (b) Same as (a) but now for the subsurface background salinity (S_{b2}).

3.2 Model behaviour

Both model set ups show three general types of yearly cycles: the water column is stable for the entire year, the water column overturns once a year, or the water column overturns twice a year. The typical yearly cycles are shown in Fig. 5 where every letter stands for a regime change, and where the different regimes are shown with different colors. The yearly cycle starts at 'A', and follows the alphabetical order. A yearly cycle ends again at 'A'.

In the stable cycle we see that the model cycles between the regimes 2 (stable, ice free) and 4 (stable, ice covered). At 'A' the regime transits from regime 2 to 4 because freezing temperature is reached. An increase in salinity is observed due to brine rejection during ice growth. The salinity decreases again when the sea ice starts to melt. At 'B' the model transits back to regime 2, because all the sea ice has melted. Due to the ocean atmospheric heat flux the temperature first rises in summer. When the ocean atmospheric heat flux switches sign, the model cools down, until freezing temperature is reached again at 'A'.

If the model overturns once, the model overturns in regime 3 (mixed, ice covered). At 'A' the model transits from regime 2 to 4, and sea ice starts to grow. After a period of sea ice growth, and subsequent brine rejection in regime 4, density increases enough to cause instability at node 'B'. At 'B' the model transits from regime 4 to 3 and overturns. The mixing of the two layers causes an increase in temperature and salinity, because the warm and salty subsurface layer is more dominant due to its larger size. At 'C' stabilisation of the water column leads to a transition back to regime 4. The sea ice is quickly melted away and regime 2 is entered at 'D'. The transition 'B-C-D' happens on the order of minutes. At node 'D' a polynya has formed. The ocean atmospheric heat flux is still negative (causing

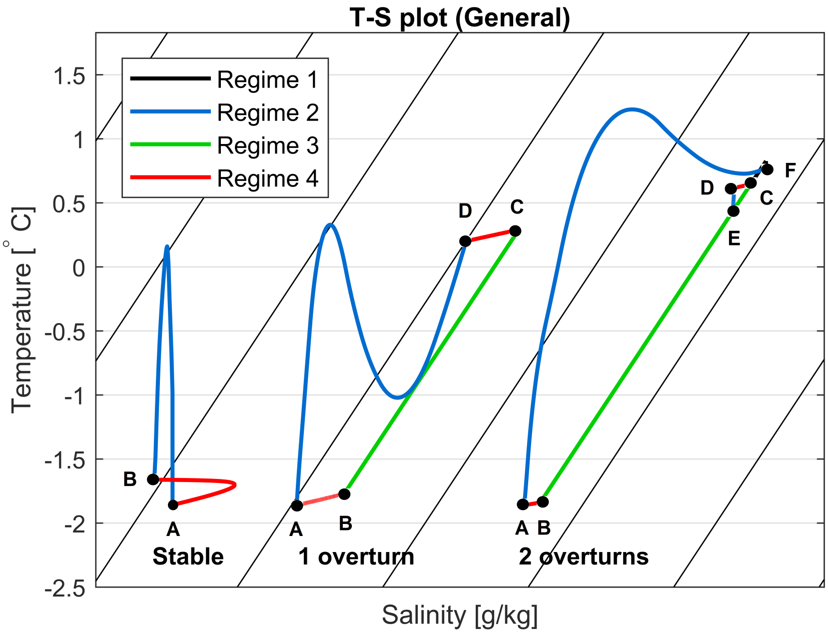

Fig. 5: T-S diagram with arbitrary scale on the salinity axis, showing three general cycles: a stable cycle (left), 1 overturn (middle), and 2 overturns each year (right). The different model regimes are displayed in black (1), blue (2), green (3), and red (4). The letters (A-F) represent regime changes. The cycle starts at A, and follows the alphabetical order. The black contour lines represent density, which increases from left to right. At freezing temperature ($T = -1.86$°C), ice grows and brine is rejected (A). In the stable cycle the ice eventually melts and regime 2 is entered (B). The other two cycles overturn in regime 3 (B to C), and transit immediately back to regime 4 (C). The ice melts and regime 2 is entered (D). In the cycle with two overturns, the model overturns again, but now in regime 1 (E), after which the model transits back to regime 2 (F). The model cools down until freezing temperature is reached and the cycle is repeated (A).

cooling), but no sea ice is present. After 'D' the model cools down in the remaining part of the winter, it warms again in the summer, and eventually cools down again until freezing temperature is reached at 'A'. This cycle is also shown in Martinson et al. (1981).

For the yearly cycle with two overturns, all four regimes are entered. Until node 'D' the behaviour is comparable with the cycle with only one overturn. Compared to the yearly cycle with only one overturn, less sea ice is formed. When regime 2 is entered at D, again a polynya has formed and the surface layer starts to cool down. Due to this cooling, the density of the surface layer increases. This causes static instability of the water column leading to an overturn at node 'E'. Regime 1 (mixed, ice free) is entered. In regime 1 the temperature and salinity remain relatively constant because the influence of the surface forcing becomes relatively smaller due to the increased depth of the surface layer (160m to 2000m). At 'F' the water column has stabilised again due to a decreasing density, and regime 2 is entered. After a warming period, the model cools down to freezing temperature at 'A', and the cycle is repeated.

3.3 Martinson set up

Using the 'Martinson' set up an attempt was made to reproduce the results of Martinson et al. (1981). Using the same model and parameter values, the produced results were different from the results in Martinson et al. (1981). In this study we use a different numerical scheme than in Martinson et al. (1981). However, using the original numerical scheme, the original results of Martinson et al. (1981) were not reproduced. A possible reason for the differences is incomplete parameter documentation. It is for instance not clear how the heat fluxes were interpolated in the model, and no numerical parameters (the time step) were given. We use a different forcing and parameter values compared to the original study based on the CESM simulation of van Westen and Dijkstra (2019). This forcing is also used for the Extended model set up. Using the same forcing for both set ups allows us to make a better comparison between the resutls of both set ups. The values used in this study are presented in the previous sections (Sections 2.2 and 3.1). Even though a different forcing and parameter values is used, the general model behaviour (Fig. 5) is comparable to the results of Martinson et al. (1981). Therefore this model set up can still be used to look into the irregularity of the polynya and the importance of surface forcing. Tests with this model set up show two stable solutions of the model: the model does not overturn at all (represented by case REF.1), or the model overturns twice each year (represented by case REF.2).

Cases REF.1 (Fig. 6) and REF.2 (Fig. 7) have been run for 100 years. The last 25 years are displayed, so no spin-up effects are present. Fig. 6 displays the results for REF.1. The density of both layers (Fig. 6a), the ice thickness (Fig. 6a), and a T-S plot (Fig. 6c) are shown. Compared to REF.2, REF.1 is the more stable case, which is also seen in the results. The model remains in the stable regimes during the entire simulation, and after the adjustment to the initial conditions (approximately 2 years for T_1 and δ and 10 years for S_1) a repeating yearly cycle is reached. This is clearly visible in the T-S plot (Fig. 6c), where the colours represent time. Only the last year is seen in the plot, since the previous years follow the same yearly cycle. The arrows represent the direction in time. The model cycles between regimes 2 (stable, ice free) and 4 (stable, ice covered), as comparable to the stable cycle of Fig. 5. No polynyas are formed in this case.

In REF.2 (Fig. 7) the diffusivity coefficient K_S, related to the salt transfer between the surface and subsurface layer, is increased to 2×10^{-6} ms^{-1} to initiate overturning of the model. Again the model reaches an repeating yearly cycle. However, in this case the yearly cycles are not exactly the same, which can be seen in the slowly decreasing (over time) sea ice thickness maxima (Fig. 7b). In the T-S plot (Fig. 7c) this effect is also seen: in regime 3 (mixed, ice covered), the last year (yellow) does not completely overlap previous

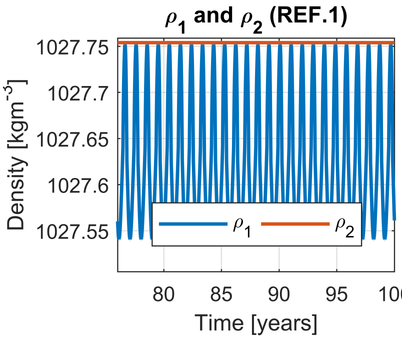

(a) *Density of both layers for case REF.1.*

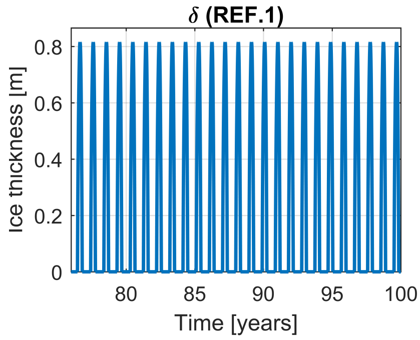

(b) *Sea ice thickness for case REF.1.*

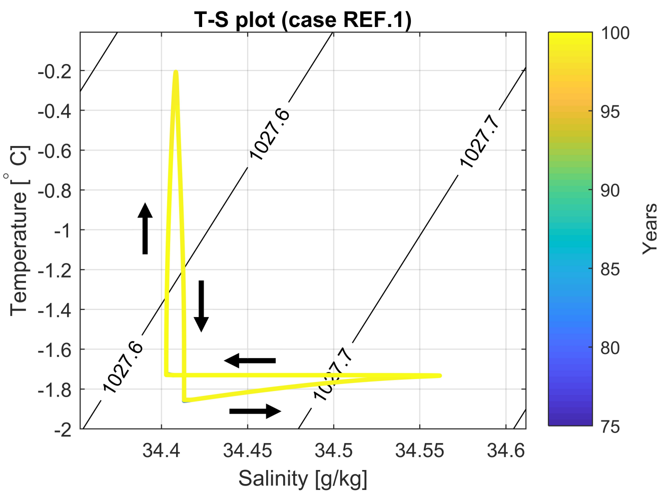

(c) *T_1-S_1 plot for case REF.1.*

Fig. 6: Years 76-100 for case REF.1 (Martinson set up with $K_S = 1.375 \times 10^{-6}$ ms^{-1}). (a) Density of the surface (blue) and subsurface (red) layer. (b) Sea ice thickness. (c) T-S plot of the temperature and salinity of the surface layer. Colouring of the lines represents time, ranging from year 76 (blue) to year 100 (yellow). Only the last year is visible, because previous years have the same yearly cycle. The black contour lines represent the density in kg m^{-3}. The arrows indicate direction in time.

years (visible by a small blue line to the right of the yellow line). The model cycles through all four regimes. Each year the model overturns twice, as seen in Fig. 7c. This cycle is comparable to the yearly cycle with two overturns in Fig. 5. A polynya is formed each year due to the overturning. This means that only one large polynya period is simulated.

These results show that the Martinson set up (no horizontal advective fluxes, constant subsurface layer) is unable to switch between a stable yearly cycle, and a cycle with one or two overturns and back again. The model has two stable solutions: either it does not overturn (Fig. 6), or it overturns twice each year (Fig. 7). This shows that to be able to simulate periodic polynya events, more physical processes need to be included. In climate models heat accumulation is shown to be important for inducing overturning , and heat

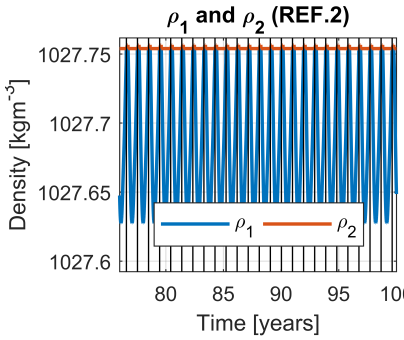

(a) Density of both layers for case REF.2.

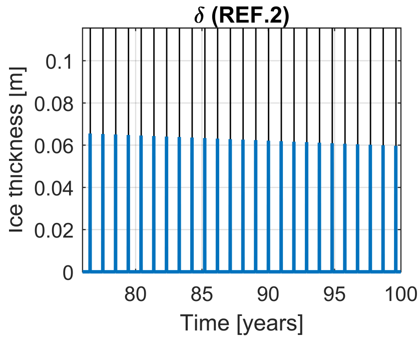

(b) Sea ice thickness for case REF.2.

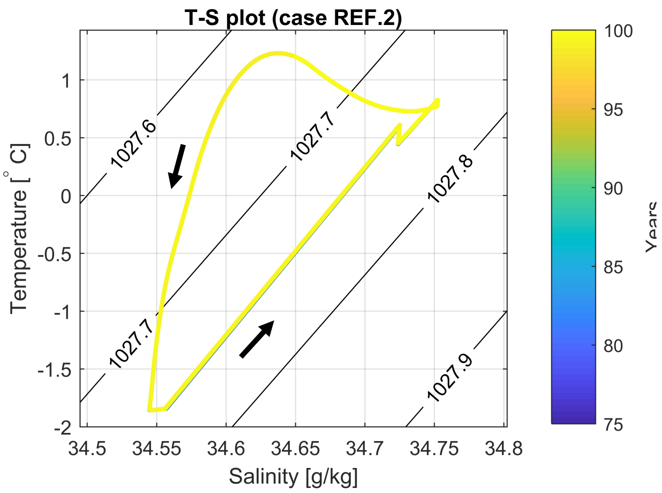

(c) T_1-S_1 plot for case REF.2.

Fig. 7: Years 76-100 for case REF.2 (Martinson set up with $K_S = 2 \times 10^{-6}$ ms^{-1}). (a) Density of the surface (blue) and subsurface (red) layer. Black lines represent overturning. (b) Sea ice thickness. Black lines represent overturning. (c) T-S plot of the temperature and salinity of the surface layer. Colouring of the lines represents time, ranging from year 76 (blue) to year 100 (yellow). Only the last year is visible, because previous years have the same yearly cycle. The black contour lines represent the density in kg m^{-3}. The arrows indicate direction in time.

depletion for stabilising the water column. These processes are not present in the Martinson set up, but they are in the Extended model set up.

3.4 Extended set up

With the inclusion of periodic subsurface forcing (Section 3.1), these additional physical processes are introduced. With this model set up, an attempt is made to reproduce the general features of van Westen and Dijkstra (2019) using a simple model. By comparing the general behaviour of the polynya events in both models, the performance of the model can be evaluated. In van Westen and Dijkstra (2019) periodic polynya events are seen, with a periodicity of 25 years. Each 25 year period has approximately 20 non-polynya years, and 5

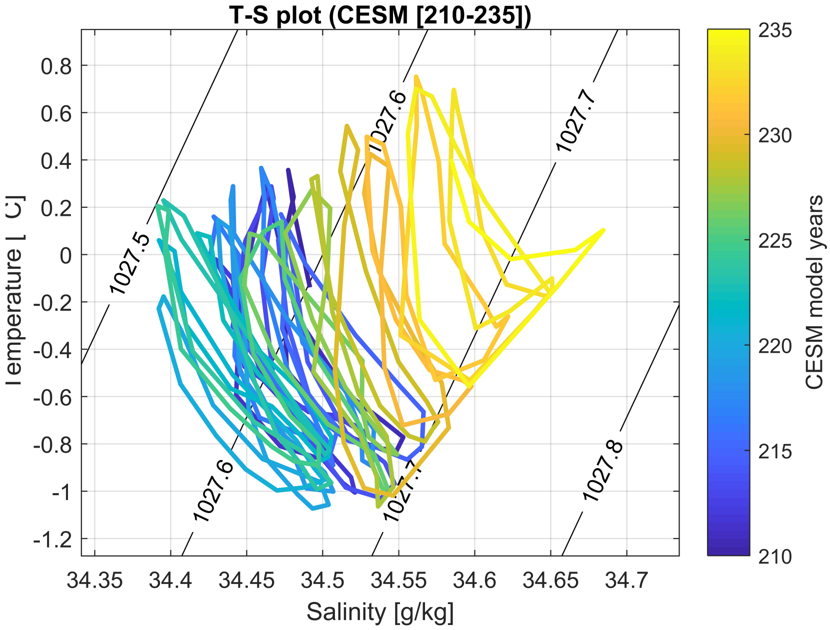

Fig. 8: T-S plot of CESM model years 210-235 from the simulation used by van Westen and Dijkstra (2019). The model is based on monthly values of the temperature and salinity averaged over the surface layer (0-160m) in the polynya region (2°E - 11°E $\times$ 63.5°S - 66.5°S) determined in van Westen and Dijkstra (2019). The colour coding represents time (year 210 is blue, year 235 is yellow). The polynya period captured in this plot is between years 231 and 235. The black contour lines represent density in kg m^{-3}, using a simple linear equation of state (Equation 5).

polynya years. The polynyas occur approximately 6 years after the subsurface heat and salt accumulation have reached their maximum. Fig. 8 displays a T-S plot of the cycle as seen in CESM, based on averaged values of the surface layer (0-160m) in the polynya region (2°E - 11°E $\times$ 63.5°S - 66.5°S). Monthly values are used, so some details are missing. Clear regime changes (from ice free to ice covered and back) as seen in Fig. 5 are averaged out in the CESM results (Fig. 8), but the general feature of salinity increase during a cooling period is seen, as well as little salinity change in the warming period. In Fig. 8 overturning is seen in years 231-235 (orange and yellow), as a strong increase in salinity and temperature. This is also seen in the general model behaviour (Fig. 5). In Fig. 8 the density contour lines are plotted using Equation 5. In CESM a non-linear equation of state is used, and processes such as diapycnal mixing are also included. This, and because only monthly values are used, explains why overturning does not follow the isopycnals in Fig. 8. The response of the surface layer to the periodic subsurface heat and salt accumulation is also seen. Both the salinity and temperature start to decrease after year 210 (dark blue), until year 221 (light blue) when they both start to increase again until in year 231 (orange) when deep convection starts, and a polynya is formed.

The three different cases (PFB, PFH, and PFS) are assessed based on whether they represent the general features seen in the CESM simulation. The results of cases PFB, PFH, and PFS are displayed in Fig. 9, 10, and 11. All cases have been run for 100 years, from which the last 25 years are shown, so no spin-up effects are presents. For each case the density of both layers, the sea ice thickness and a T-S plot of the surface layer are given.

In case PFB (Fig. 9) heat and salt subsurface fluxes are used. Based on the fitted subsurface fluxes (Fig. 4), and Equation 5, the effects of the background subsurface temperature and salinity on the density almost compensate each other. There is a very small subsurface density maximum in the middle of a 25 year cycle (red line Fig. 9a). The cycle shown in Fig. 9 is repeated every 25 years, which means periodic polynya events are simulated. In case PFB the asymmetery between non-polynya years versus polynya years is 7 versus 18 years. These polynyas are clearly visible by reduced sea ice thickness and by reduced time that sea ice is present (Fig. 9b). In a 25 year cycle, the first overturn after a non-polynya period, occurs approximately 4 years after the subsurface heat and salt accumulation have reached their maximum. These subsurface processes also influence the characteristics of the surface layer (Fig. 9c). In cases REF.1 and REF.2 the yearly cycles overlap each other, but in this case the yearly cycles are different as a response to the subsurface heat and salt accumulation which is also seen in the CESM simulation (Fig. 8).

Where PFB uses both subsurface fluxes (heat and salt), PFH (Fig. 10) uses only a subsurface heat flux. Where PFB shows a small subsurface density maximum in the middle of the cycle, PFH shows a subsurface density minimum (red line Fig. 10a). PFH shows comparable results as in case PFB. The same dominant 25 year period for the repeating cycle is found, and the response of the surface layer characteristics to the subsurface heat accumulation is also seen (Fig. 10c). However, there are also some differences. Where case PFB spends more time in the polynya regime, case PFH spends the same time in both regimes (non-polynya and polynya). The first overturn after a non-polynya period occurs approximately 3 years before the subsurface heat accumulation maximum, where in case PFB this was 4 years after(!) the maximum. In case PFB the subsurface density has a maximum in the middle of the plotted period (around year 87.5 in the red line in Fig. 9a), where case PFH has a subsurface density minimum at this time (red line Fig. 10a). This is because heat accumulation results in buoyancy gain in both cases, but in case PFB this buoyancy gain is compensated by densification due to salt accumulation. In Fig. 10a overturning occurs because the density of the subsurface layer decreases, where as in Fig. 9a this clear relation is not visible.

In case PFS (Fig. 11) only a salt subsurface flux is used. As a response to the subsurface salt accumulation, the subsurface density has a maximum in the middle of the plotted temperature (red line at 87.5 years in Fig. 11a). This maximum is larger compared to the subsurface density maximum of case PFB. Just as cases PFB and PFH, case PFS has a dominant period of 25 years for the repeating cycle. The response to the subsurface salt accumulation in the surface characteristics (Fig. 11c) is comparable to the responses seen in PFB (Fig. 9a), PFH (Fig. 10a), and CESM (Fig. 8). The differences with respect to PFB are the time spend in a polynya period each cycle, and the time when the first overturn occurs after a non-polynya period. Case PFS spends more time (11 years) in the non-polynya period relative to PFB (7 years). The first overturn occurs approximately 8 years after the subsurface density maximum as a response to a decreasing density of the subsurface layer. Another important difference is the response of the sea ice thickness during a non-polynya period to the subsurface forcing. The sea ice thickness in case PFB responds to the subsurface heat accumulation (Fig. 9b). In case PFS there is no subsurface heat accumulation, resulting in a constant sea ice thickness maximum during the non-polynya period (Fig. 11b).

All cases are able to simulate the general features also seen in the CESM simulation of van Westen and Dijkstra (2019). All cases show a repeating 25 year cycle, which is the same period as the period of the subsurface forcing and the same period as seen in CESM. Where CESM has more non-polynya years than polynya years, cases PFB and PFS have more polynya years, and case PFH has as many non-polynya years as polynya years. Besides this difference, also the timing of the first overturn after a non-polynya period is different with respect to CESM. In CESM the first overturn occurs approximately 6 years after the subsurface heat and salt accumulation have reached their maximum. PFB overturns 2 years earlier, and PFS 2 years later. Case PFH differs most, since it overturns 9 years earlier, and even before the subsurface heat accumulation has reached its maximum. These differences are probably caused by the simplicity of the model, and most likely due to the representation of mixing in this model compared to CESM. Since all cases represent the general features of the CESM simulation, it is not possible to determine a case which performs best. However, looking at observations (Fahrbach et al., 2011), and also model results of van Westen and Dijkstra (2019), heat and salt accumulation are seen. This heat and salt accumulation are only present in case PFB, suggesting case PFB is physically most complete.

3.5 Addition of noise

In the previous two sections we have seen that only the Extended model set up simulates multiple polynya events. The period of the polynya events equals the the period of the subsurface forcing. In this section I will test whether this period is still dominant under the influence of noise. To this end, white noise is added to the freshwater flux to include

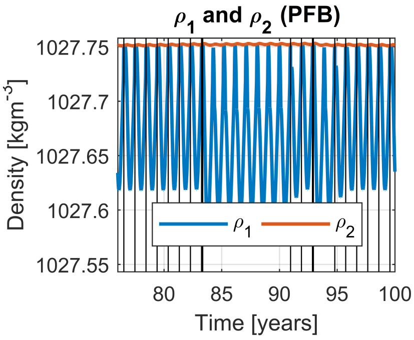

(a) Density of both layers for case PFB.

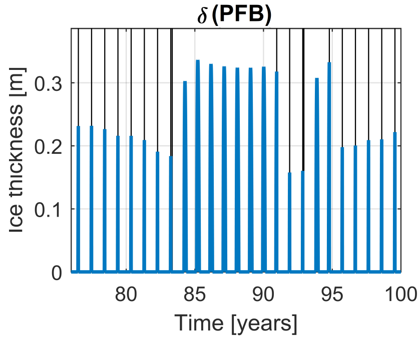

(b) Sea ice thickness for case PFB.

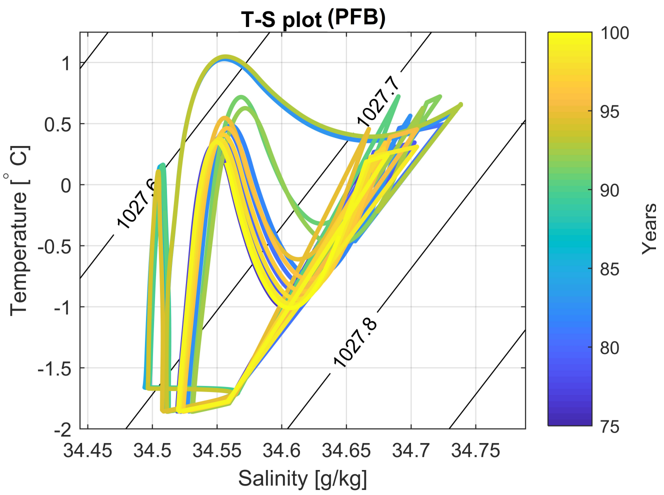

(c) T_1-S_1 plot for case PFB.

Fig. 9: Years 76-100 for case PFB ('Extended' model set up with both subsurface fluxes). (a) Density of the surface (blue) and subsurface (red) layer. Black lines represent overturning. (b) Sea ice thickness. Black lines represent overturning. (c) T-S plot of the temperature and salinity of the surface layer. Colouring of the lines represents time, ranging from year 76 (blue) to year 100 (yellow). The black contour lines represent the density in kg m^{-3}.

density anomalies in the surface layer related to the natural variability of the precipitation and evaporation in this region. This has been done for case PFB. Case REF.1 has also been tested with noise, to see if noise can force the model in different polynya regimes. The mean freshwater flux has been determined in Section 3.1. From the CESM simulation of van Westen and Dijkstra (2019) a signal-to-noise ratio ($SNR = \frac{\mu^2}{\sigma^2} = 4.07$) was determined. Using this signal-to-noise ratio, a white noise signal was determined and added to the freshwater flux (F). Case REF.1 has also been run with a signal-to-noise ratio of 0.1. For both cases 100 year runs were performed, from which the first 25 years were removed to exclude spin up effects. 100 ensemble members are used to ensure a robust analysis.

Fig. 12 displays the spectral analysis on the variables T_1 (Fig. 12a), S_1 (Fig. 12b), and δ (Fig. 12c) for case PFB. In the figure the 10$^{\text{th}}$ and 90$^{\text{th}}$ percentile are plotted, as well as

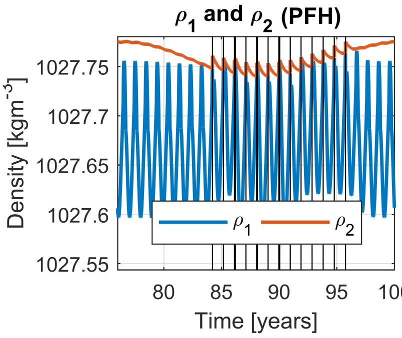

(a) Density of both layers for case PFH.

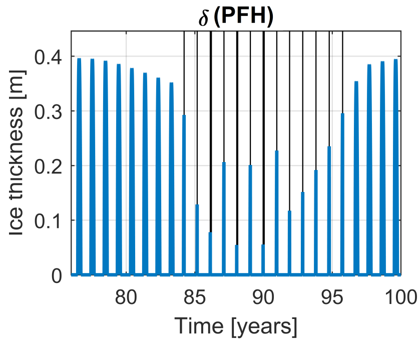

(b) Sea ice thickness for case PFH.

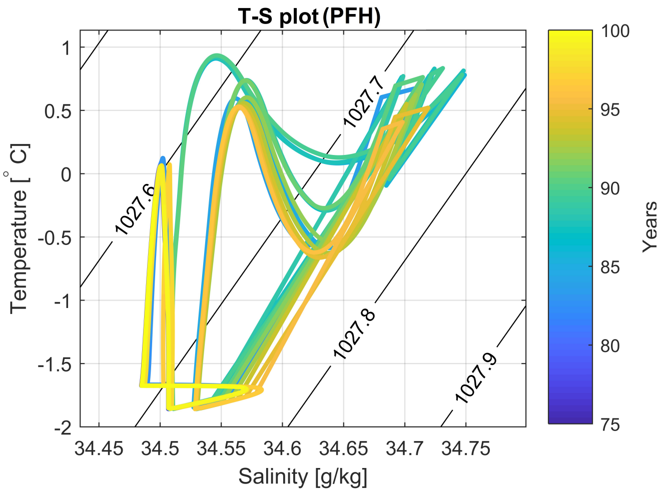

(c) T_1-S_1 plot for case PFH.

Fig. 10: Years 76-100 for case PFH ('Extended' model set up with only a subsurface heat flux). (a) Density of the surface (blue) and subsurface (red) layer. Black lines represent overturning. (b) Sea ice thickness. Black lines represent overturning. (c) T-S plot of the temperature and salinity of the surface layer. Colouring of the lines represents time, ranging from year 76 (blue) to year 100 (yellow). The black contour lines represent the density in kg m^{-3}.

the mean of all runs, the median, and a randomly chosen run. For all variables a dominant period of 25 years is visible, the same period as the subsurface forcing. This period is most dominant for the surface layer temperature (Fig. 12a). For the longer periods, the integrated effect of the white noise (red noise processes) becomes visible. This figure shows that the dominant period of 25 years is still visible with the inclusion of noise.

In Fig. 13 the spectral analysis of T_1 (Fig. 13a), S_1 (Fig. 13b), and δ (Fig. 13c) are plotted, but now for case REF.1. REF.1 initially did not simulate overturning. The inclusion of noise does result in overturning in REF.1. However, no clear dominant period is found. Analysis of the different runs indicates that using a signal-to-noise ratio of 4.07, the model cannot be forced from a polynya period to a non-polynya period. The noise only affects the timing of the first overturn. With a smaller SNR (0.1), the same applies: once

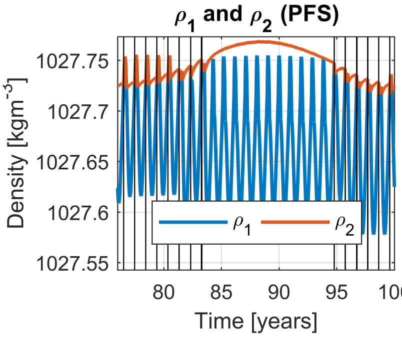

(a) Density of both layers for case PFS.

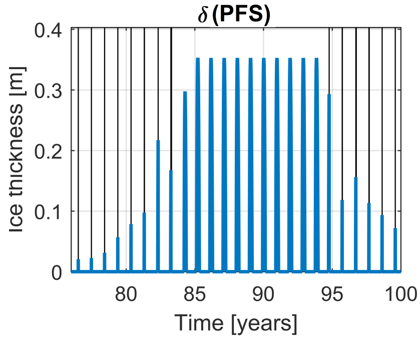

(b) Sea ice thickness for case PFS.

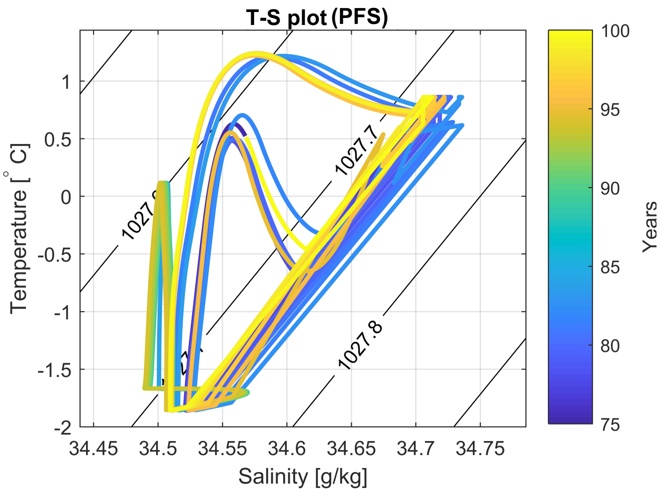

(c) T_1-S_1 plot for case PFS.

Fig. 11: Years 76-100 for case PFS ('Extended' model set up with only a subsurface salt flux). (a) Density of the surface (blue) and subsurface (red) layer. Black lines represent overturning. (b) Sea ice thickness. Black lines represent overturning. (c) T-S plot of the temperature and salinity of the surface layer. Colouring of the lines represents time, ranging from year 76 (blue) to year 100 (yellow). The black contour lines represent the density in kg m^{-3}.

the model is in a polynya period, it is stuck in this period. The model is unable to switch back to a non-polynya period. This was also seen in the results of REF.2 without noise (Fig. 7).

4 Summary and discussion

The Weddell Polynya is a hole in the sea ice in the Southern Ocean. The Weddell Polynya is caused by deep convection (Martinson et al., 1981), but there is no consensus on how this deep convection is induced. Studies have looked into atmospheric processes (e.g. Martinson et al., 1981; Gordon et al., 2007; Francis et al., 2019), dynamical processes (e.g. Holland, 2001; Kurtakoti et al., 2018), and subsurface processes (e.g van Westen and Dijkstra, 2019).

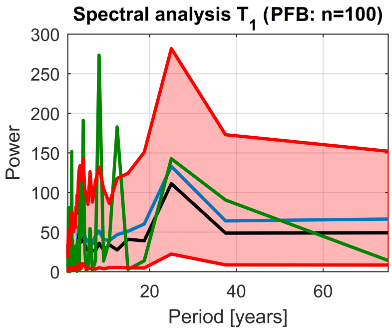

(a) Spectral analysis T_1, case PFB.

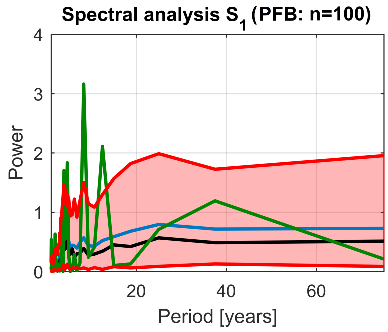

(b) Spectral analysis S_1, case PFB.

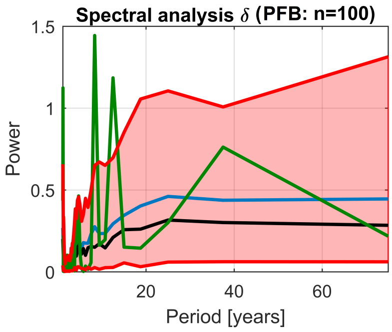

(c) Spectral analysis δ, case PFB.

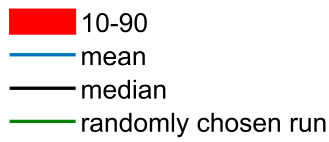

Fig. 12: Spectral analysis for variables (a) T_1, (b) S_1, and (c) δ (c) for case PFB ('Extended' model set up with both subsurface fluxes). The analysis is based on 100 ensemble members. Each ensemble member contains the last 75 years of a 100 year run to exclude spin up effects. The red band represents the ensemble members between the 10^{th} and 90^{th} percentile. Also the mean (blue), median (black) and a randomly chosen run (green) are displayed.

The atmospheric and dynamical processes describe densification of the surface layer without a clear dominant period. High resolution climate models show periodic heat accumulation in the subsurface layer, resulting in buoyancy gain of the subsurface layer, and eventually periodic polynya events. This contrast is the base of this study. In this study the contrast between the conclusions of the study of Martinson et al. (1981) (an irregular polynya caused by brine rejection) and the conclusions of the study of van Westen and Dijkstra (2019) (a periodic polynya caused by subsurface heat accumulation) was investigated. Using a new convective model, based on the model by Martinson et al. (1981), the irregularity/periodicity of the polynya was investigated, as well as the importance of subsurface heat and salt accumulation versus brine rejection. Two different model set ups were used. Firstly, the Martinson set up, based on the original Martinson model was used to see whether the original results could be reproduced. Two cases were used (REF.1 and REF.2). I also investigated the long term behaviour of this set up to see whether multiple polynya events (e.g. the 1970s and 2017 events) could be explained. Secondly, the new convective model (Fig. 3 was used in the Extended model set up. In this set up the Martinson model is extended with

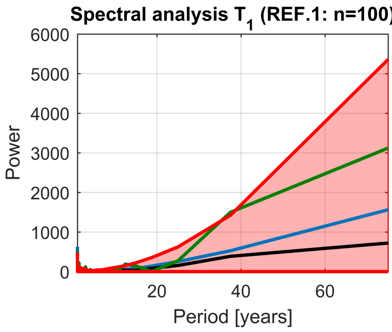

(a) *Spectral analysis T_1, case REF.1.*

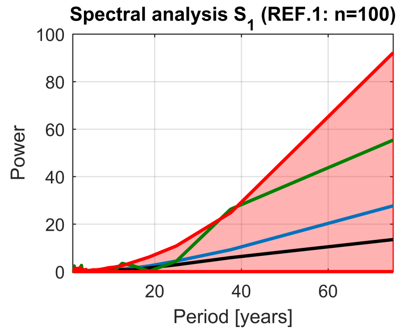

(b) *Spectral analysis S_1, case REF.1.*

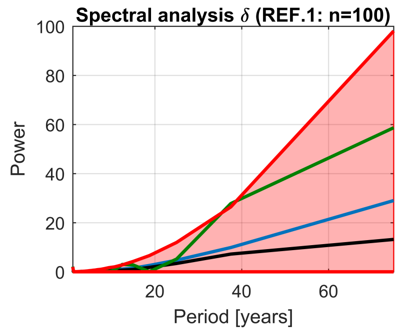

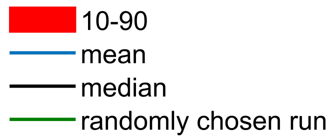

(c) *Spectral analysis δ, case REF.1.*

Fig. 13: Spectral analysis for variables (a) T_1, (b) S_1, and (c) δ for case REF.1 ('Martinson' set up with $K_S = 1.375 \times 10^{-6}\text{ms}^{-1}$). The analysis is based on 100 ensemble members. Each ensemble member contains the last 75 years of a 100 year run to exclude spin up effects. The red band represents the ensemble members between the 10^{th} and 90^{th} percentile. Also the mean (blue), median (black) and a randomly chosen run (green) are displayed.

horizontal advective fluxes in both layers, and a dynamic subsurface layer. The subsurface advective flux is periodic of nature with a period of 25 years. The main goal for this set up was to investigate the periodic behaviour of polynya events as a response to the subsurface forcing. Also the importance of the different components of the subsurface forcing was tested (cases PFB, PFH, and PFS). Lastly, white noise was added to the freshwater flux for two cases (REF.1 and PFB). The main goal for REF.1 was to see whether multiple polynya events could be simulated. For PFB the main goal was to determine how dominant the periodicity was under the influence of noise. This research indicates that the original model (Martinson set up) is not suitable to simulate multiple polynya events, which indicates that some physical processes are missing in the model. The inclusion of subsurface forcing, as suggested in van Westen and Dijkstra (2019) (Extended model set up), made it possible to simulate periodic polynya events. The dominant period for polynya events equals the dominant period of the subsurface forcing. This same period was still seen with the addition of white noise to the freshwater flux. Addition of noise to the original Martinson model did not result in multiple polynya events.

In this study I tried to reproduce the results of Martinson et al. (1981) using the Martinson set up to try to verify their conclcusions. Their exact results were not reproduced, but the general model behaviour was the same. The timing of the first overturn was for example earlier with respect to the results in Martinson et al. (1981). The reason why the exact results were not reproduced is probably missing information in the parameter documentation. It is for instance not clear how the monthly heat fluxes were interpolated in the model. Different interpolation techniques have been used, but still, the timing of the first overturn differed with respect to Martinson et al. (1981). Another missing parameter is the used time step. Relatively small time steps have been used, but still differences were found. Therefore it is also possible some parameter values were documented incorrectly. Even though the exact results were not reproduced, the general behaviour of the model used in this study was the same as described in Martinson et al. (1981). Therefore the model was still used, however a different forcing, and different parameter values were used (cases REF.1 and REF.2). With these cases an attempt was made to verify the conclusions of Martinson et al. (1981).

The first conclusion of Martinson et al. (1981) was that the deep convection is caused by brine rejection in a preconditioned surface layer. In this model, deep convection starts after a short period of sea ice growth and subsequent brine rejection. Brine rejection causes a rapid increase of density in the surface layer. The results (Fig. 7) clearly show that this eventually triggers the deep convection. However, brine rejection alone cannot explain multiple polynya events (e.g. the 1970s and 2017 events), since brine rejection is present in all years with sea ice growth, and not all years show deep convection and subsequent polynya formation (Fig. 6).

The second conclusion of Martinson et al. (1981) was that the WP is an irregular event. Based on my tests with the same model, I have shown that the original model is incapable of simulating multiple events. The model has two stable solutions, it either does not overturn (case REF.1, Fig. 6), or it does overturn each year (case REF.2, Fig. 7). In Martinson et al. (1981) it was also shown that when the cycle becomes stable, it will remain stable, either in regimes 2 (ice free, stable) and 4 (ice covered, stable), or in regimes 1 (ice free, mixed) and 2 (ice free, stable). The first stable solution (regimes 2 and 4) can be explained by a too strong stratification. In case REF.1 the salt transfer (governed by K_S) of the subsurface layer to the surface layer is too weak to break the stratification. In the second stable solution (regimes 1 and 2) this salt transfer is increased, which causes instability in the water column with mixing as a result. The model will overturn each year and no stable cycle is reached. In climate models the water column stabilises after deep convection when the heat and salt reservoirs are depleted. This depletion leads to stabilisation of the water column by increasing the density of the subsurface layer through heat depletion. This physical process is missing in the Martinson set up, and therefore the model is not able return to a non-polynya regime. However, in Martinson et al. (1981) it was possible to simulate polynyas followed by a stable, non-overturning regime. The model overturns in the first years, after which a stable, non-polynya cycle is simulated. These overturns in the first years are caused by the initial conditions. When the model is adjusted to the forcing, the stable state is achieved. My results thus correspond well to the model analysis in Martinson et al. (1981). Irregularity does not occur, because the model becomes stable after a few years and only one event can be simulated.

The Extended model set up was used to look into the conclusions of van Westen and Dijkstra (2019), and to compare the results of this set up to the results of the Martinson set up. Three cases were used: periodic flux both (PFB, Fig. 9), periodic flux heat (PFH, Fig. 10), and periodic flux salt (PFS, Fig. 11). van Westen and Dijkstra (2019) concluded that the WP is a regular, periodic event, with a dominant period of 25 years. This dominant period is attributed to periodic subsurface heat and salt accumulation related to the SOM mechanism. In my extended model this periodic subsurface heat and salt accumulation is represented by a periodic heat and salt flux in the subsurface layer. The results (Fig. 9 to 11) showed periodic polynya events with the same dominant period as seen in van Westen and Dijkstra (2019) caused by the periodic subsurface forcing. This is in contrast with the conclusion of Martinson et al. (1981) that the polynya is an irregular event. However, the conclusions of Martinson et al. (1981) are based on a model that is unable to simulate multiple events, and is not forced by a periodic subsurface forcing. This suggests that under the influence of periodic subsurface forcing, the polynya is a periodic event. It is therefore possible that periodic subsurface forcing is the missing physical process in the Martinson set up.

van Westen and Dijkstra (2019) also suggested that deep convection is caused by instabilities in the subsurface layer due to the accumulation of heat. In the extended model the influence of the subsurface forcing on the stratification could be seen (Fig 9 to 11). The subsurface forcing preconditions both the subsurface and the surface layer, after which a density increase in the surface layer due to brine rejection triggers the deep convection. This conclusion extends the conclusion of Martinson et al. (1981). The results of both model set ups (Martinson and Extended) suggest that brine rejection alone is not sufficient to explain multiple polynya events. The inclusion of periodic subsurface forcing does make that possible. The conclusion of van Westen and Dijkstra (2019) that the subsurface heat flux is more dominant than the subsurface salt flux has not been confirmed, since all extended model cases (PFB, PFH, and PFS) show comparable behaviour. However, looking at the equations of the model (Equations 1 to 5), the subsurface heat flux has the largest impact on the results. The subsurface heat flux influences (some indirectly) every quanity (T_2, ρ_2, T_1, ρ_1, δ, S_1, S_2) in the model. The subsurface salt flux affects the density and salinity of both layers, and therefore has a much smaller influence on the results.

The extended model was able to capture the general features as seen in van Westen and Dijkstra (2019). However, the model is still too idealised to accurately reproduce all features in the CESM simulation. The asymmetry in the non-polynya regime versus the polynya regime was poorly resolved. This is probably due to the difference in how overturning is resolved. In this model the layers are either in stable stratification with a constant layer depth, or they are completely mixed. In van Westen and Dijkstra (2019), a KPP boundary mixed layer scheme is used. Resolving the growth of the mixed layer more accurately would improve the model, and possibly lead to a better representation of the asymmetry between the two regimes. When the mixed layer is allowed to grow more gradually, a lag is introduced in the system. This will delay the formation of a polynya. Due to this instant mixing, both temperature and salinity in the surface layer increase instantly. This results in large differences after overturning between my results and the CESM simulation of van Westen and Dijkstra (2019). Other important differences between the two models are the representation of the atmospheric and dynamical processes. In my model these processes are either prescribed (e.g. freshwater input), parameterised (e.g. upwelling) or absent (e.g. the wind field). However, even though the model is simplistic, important features were simulated. Seasonality in the yearly cycle was observed, as well as the effects of sea ice growth and melt on the surface salinity. Periodic polynya events were simulated with the same period as the subsurface forcing. And lastly, the periodic nature of the subsurface layer was seen through heat and salt transfer in the surface layer. This shows that even though not all physical processes are present in the model, the most important processes are either present or captured by good parameterisations.

My extended model is forced by periodic subsurface fluxes attributed to the SOM, an intrinsic dynamical ocean mode in the Southern Ocean. This mode is mainly caused by interaction between eddies and the mean flow (Jüling et al., 2018). The SOM leads to ocean heat content anomalies in the South Atlantic Ocean. These anomalies propagate with the ACC to 30°E where they enter the Weddell Gyre as WDW. Propagating along the ambient current, the anomalies eventually reach the Maud Rise region. Positive heat content anomalies lead to heat accumulation in the subsurface layer, and eventually an unstable stratification, resulting in deep convection which is forced from below. This heat accumulation can induce deep convection, releasing the subsurface heat. In van Westen and Dijkstra (2019) the period of the polynya events was attributed to the period of the

SOM, which is 25 years. In my extended model, subsurface fluxes related to this heat accumulation were used. The used period for the fluxes equals the periodicity of the polynya events. The results of this study suggest that periodicity in polynya events could be caused by periodicity in the subsurface heat and salt accumulation which van Westen and Dijkstra (2019) attribute to the SOM. However, it is also possible that the Weddell Polynya has a feedback on the SOM itself, but due to the simplicity of the model, it was not possible to assess this in this study.

The SOM is used to explain the period in the study of van Westen and Dijkstra (2019). However, several climate models show irregular polynya events with no clear preferred period (e.g. Martin et al., 2013; Zhang and Delworth, 2016; Reintges et al., 2017). This can be explained by the resolution of the model. Low resolution models are unable to capture the eddies that are crucial for the SOM. Therefore the SOM is not resolved. Heat accumulation is still seen in these models (e.g. in the low resolution run of Dufour et al, 2017), but this is not related to the SOM mechanism, and therefore has not the same dominant period (van Westen and Dijkstra, 2019). Another effect of a lower resolution, is a weaker stratification (Dufour et al., 2017). A weaker stratification leads to a system that is more sensitive to density anomalies. These anomalies can originate from anomalies in for instance the freshwater input, surface heat fluxes and subsurface fluxes. Density anomalies can induce deep convection. Without a dominant periodic forcing, in a more sensitive system, the period of deep convection becomes more irregular, which is seen in low resolution models.

In this study I looked at the importance of the subsurface forcing relative to the surface forcing. Some studies point to surface processes as the cause of deep convection in a preconditioned ocean (e.g. Martinson et al., 1981). More recent studies also investigated surface processes such as a cyclone (Francis et al., 2019), and advection of warm-moist air in combination with increased upwelling due to a favourable wind stress curl (Jena et al., 2019). However, studies using climate models show the importance of heat accumulation in the subsurface layer (e.g Reintges et al., 2017). My study, in combination with the study of van Westen and Dijkstra (2019), shows that subsurface accumulation of heat is one of the main drivers of the WP. Brine rejection is an important process to cause density anomalies in the surface layer. However, in this model this is not the most dominant process, since it cannot explain the periodic return of the polynya in my model and in observations. Other surface processes, such as strong cyclones (Francis et al., 2019), eddy shedding at Maud Rise (Holland, 2001), and Taylor cap dynamics (Kurtakoti et al., 2018) are not unimportant. These effects in the Maud Rise region can be important for the duration, location, and size of the polynya. However, I suggest that subsurface processes govern the initial formation and periodicity of the Weddell Polynya.

References

Alverson, K., Owens, W.B., 1996. Topographic Preconditioning of Open-Ocean Deep Convection. J. Phys. Oceanogr. 26, 2196–2213. doi:10.1175/1520-0485(1996)026<2196:TPOOOD>2.0.CO;2.

Carsey, F.D., 1980. Microwave Observations of the Weddell Polynya. Mon. Weather Rev. 108, 2032–2044. doi:10.1175/1520-0493(1980)108<2032:MOOTWP>2.0.CO;2.

Cheon, W.G., Gordon, A.L., 2019. Open-ocean polynyas and deep convection in the Southern Ocean. Sci. Rep.-UK 9. doi:10.1038/s41598-019-43466-2.

Dufour, C.O., Morrison, A.K., Griffies, S.M., Frenger, I., Zanowski, H., and co-authors, 2017. Preconditioning of the Weddell Sea polynya by the ocean mesoscale and dense water overflows. J. Climate 30, 7719–7737. doi:10.1175/JCLI-D-16-0586.1.

Fahrbach, E., Hoppema, M., Rohardt, G., Boebel, O., Klatt, O., and co-authors, 2011. Warming of deep and abyssal water masses along the Greenwich meridian on decadal time scales: The Weddell gyre as a heat buffer. Deep-Sea Res. Pt. II 58, 2509–2523. doi:10.1016/j.dsr2.2011.06.007.

Francis, D., Eayrs, C., Cuesta, J., Holland, D., 2019. Polar cyclones at the origin of the reoccurrence of the Maud Rise Polynya in austral winter 2017. J. Geophys. Res. 0. doi:10.1029/2019JD030618.

Gordon, A.L., Viscbeck, M., Comiso, J.C., 2007. A Possible Link between the Weddell Polynya and the Southern Annular Mode. J. Climate 20, 2258–2571. doi:10.1175/JCLI4046.1.

Holland, D.M., 2001. Explaining the Weddell Polynya - a Large Ocean Eddy Shed at Maud Rise. Science 292, 1697–1700. doi:10.1126/science.1059322.

Jena, B., Ravichandran, M., Turner, J., 2019. Recent Reoccurrence of Large Open-Ocean Polynya on the Maud Rise Seamount. Geophys. Res. Lett. 46, 4320–4329. doi:10.1029/2018GL081482.

Jüling, A., Viebahn, J.P., Drijfhout, S.S., Dijkstra, H.A., 2018. Energetics of the Southern Ocean Mode. J. Geophys. Res. 123, 9283–9304. doi:10.1029/2018JC014191.

Klatt, O., Fahrbach, E., Hoppema, M., Rohardt, G., 2005. The transport of the Weddell Gyre across the Prime Meridian. Deep-Sea Res. Pt. II 52, 513–528. doi:https://doi.org/10.1016/j.dsr2.2004.12.015.

Klopfenstein, R.W., 1971. Numerical differentiation formulas for stiff systems of ordinary differential equations. RCA Rev. 32, 447–462.

Kurtakoti, P., Veneziani, M., Stössel, A., Weijer, W., 2018. Preconditioning and Formation of Maud Rise Polynyas in a High-Resolution Earth System Model. J. Climate 31, 9659–9678. doi:10.1175/JCLI-D-18-0392.1.

Latif, M., Martin, T., Reintges, A., Park, W., 2017. Southern Ocean Decadal Variability and Predictability. Curr. Clim. Change Rep. 3, 163–173. doi:10.1007/s40641-017-0068-8.

de Lavergne, C., Palter, J.B., Galbraith, E.D., Bernardello, R., Marinov, I., 2014. Cessation of deep convection in the open Southern Ocean under anthropogenic climate change. Nat Clim Chang. 4, 278. doi:10.1038/NCLIMATE2132.

Le Bars, D., Viebahn, J.P., Dijkstra, H.A., 2016. A Southern Ocean mode of multidecadal variability. Geophys. Res. Lett. 43, 2102–2110. doi:10.1002/2016GL068177.

Lindsay, R.W., Holland, D.M., Woodgate, A., 2004. Halo of low ice concentration observed over the Maud Rise seamount. Geophys. Res. Lett. 3, 1–4. doi:10.1029/2004GL019831.

Martin, T., Park, W., Latif, M., 2013. Multi-centennial variability controlled by Southern Ocean convection in the Kiel Climate Model. Clim. Dynam. 40, 2005–2022. doi:10.1007//s00382-012-1586-7.

Martinson, D.G., Killworth, P.D., Gordon, A.L., 1981. A Convective Model for the Weddell Polynya. J. Phys. Oceanogr. 11, 466–488. doi:10.1175/1520-0485(1981)011<0466:ACMFTW>2.0.CO;2.

Moore, G.W.K., Alverson, K., Renfrew, I.A., 2002. Local atmospheric response to an open-ocean polynya in a high-resolution climate model. J. Climate 32, 1685–1698. doi:https://doi.org/10.1175/1520-0485(2002)032<1685:AROTAS>2.0.CO;2.

Parkinson, C.L., 1983. On the Development and Cause of the Weddell Polynya in a Sea Ice Simulation. J. Phys. Oceanogr. 13, 501–511. doi:10.1175/1520-0485(1983)013<0501:OTDACO>2.0.CO;2.

Reintges, A., Martin, T., Latif, M., Park, W., 2017. Physical controls of Southern Ocean deep-convection variability in CMIP5 models and the Kiel Climate Model. Geophys. Res. Lett. 44, 6951–6958. doi:10.1002/2017GL074087.

Shaw, W.J., Stanton, T.P., 2014. Dynamic and Double-Diffusive Instabilities in a Weak Pycnocline. Part I: Observations of Heat Flux and Diffusivity in the Vicinity of Maud Rise, Weddell Sea. J. Phys. Oceanogr. 44, 1973–1991. doi:10.1175/JPO-D-13-042.1.

Wang, Z., Wu, Y., Lin, X., Liu, C., Xie, Z., 2017. Impacts of open-ocean deep convection in the Weddell Sea on coastal and bottom water temperature. Clim. Dynam. 48, 2967–2981. doi:10.1007/s00382-016-3244-y.

Weijer, W., Veneziani, M., Stössel, A., Hecht, M.W., Jeffery, N., and co-authors, 2017. Local atmospheric response to an open-ocean polynya in a high-resolution climate model. J. Climate 30, 1629–1641. doi:10.1175/JCLI-D-16-0120.1.

van Westen, R.M., Dijkstra, H.A., 2017. Southern Ocean origin of multidecadal variability in the North Brazil Current. Geophys. Res. Lett. 44, 10541–10548. doi:10.1002/2017GL074815.

van Westen, R.M., Dijkstra, H.A., 2019. Mechanisms of Multidecadal Variability in the Southern Ocean. Submitted .

Zhang, L., Delworth, T.L., 2016. Impact of the Antarctic bottom water formation on the Weddell Gyre and its northward propagation characteristics in GFDL CM2.1 model. J. Geophys. Res. 121, 5825–5846. doi:10.1002/2016JC011790.

A Regime transitions

In this appendix the mathematical representation of the regime are shown. A regime transition changes the initial conditions for the new regime. The new initial conditions are indicated with a prime. Horizontal bars above a variable represent averaging over the water column due to overturning: $\bar{X} = (hX_1 + (H-h)X_2)/H$, where X is either T or S.

$$\text{regime 1} \rightarrow \text{regime 2 when } -\alpha\tfrac{dT}{dt} + \beta\tfrac{dS}{dt} < 0;$$
$$T_1' = T,\ S_1' = S,\ \delta' = 0;$$
$$\text{regime 1} \rightarrow \text{regime 3 when } T = T_f;$$
$$T' = T_f,\ S' = S,\ \delta' = 0;$$
$$\text{regime 2} \rightarrow \text{regime 1 when } \rho_1 = \rho_2;$$
$$T' = \bar{T},\ S' = \bar{S},\ \delta' = 0;$$
$$\text{regime 2} \rightarrow \text{regime 4 when } T_1 = T_f;$$
$$T_1' = T_1,\ S_1' = S_1,\ \delta' = 0;$$
$$\text{regime 3} \rightarrow \text{regime 1 when } \delta = 0;$$
$$T' = T,\ S' = S,\ \delta' = 0;$$
$$\text{regime 3} \rightarrow \text{regime 4 when } -\alpha\tfrac{dT}{dt} + \beta\tfrac{dS}{dt} < 0;$$
$$T_1' = T,\ S_1' = S,\ \delta' = \delta;$$
$$\text{regime 4} \rightarrow \text{regime 2 when } \delta = 0;$$
$$T_1' = T_1,\ S_1' = S_1,\ \delta' = 0;$$
$$\text{regime 4} \rightarrow \text{regime 3 when } \rho_1 = \rho_2;$$
$$T' = \bar{T},\ S' = \bar{S},\ \delta' = \delta;$$

B CESM analysis

In this appendix plots determined from the data of the CESM simulation of van Westen and Dijkstra (2019) are shown. These plots are used to determine parameter values (H in Fig. 15 and h in Fig. 14), and the surface forcing (F in Fig. 17, and Q_{oa} and Q_{ia} in Fig. 16).

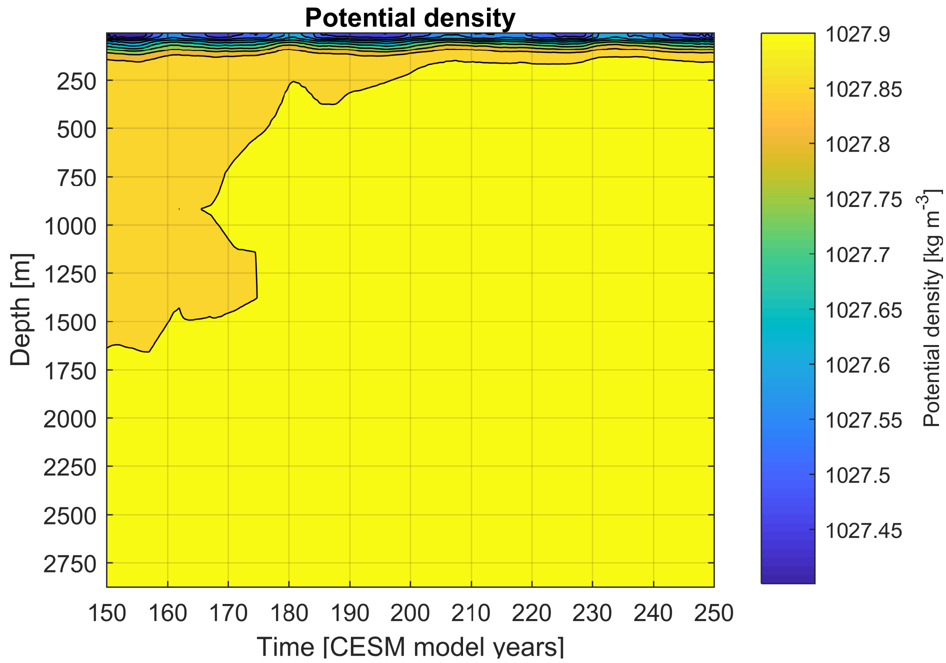

Fig. 14: Potential density over depth for CESM model years 150-250 from the CESM simulation of van Westen and Dijkstra (2019). The data has been smoothed with a 5 year moving average. A layer of approximately constant potential density forms below 160m. This 160m is taken as the depth of the surface layer (h).

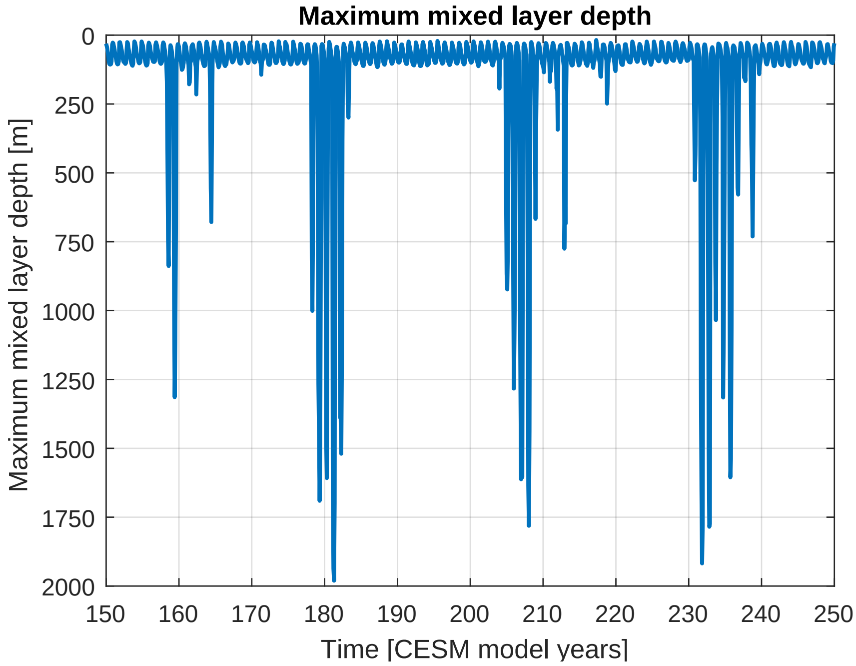

Fig. 15: The maximum mixed layer depth for CESM model years 150-250 determined from the CESM simulation of van Westen and Dijkstra (2019). The maximum mixed layer depth is of the order on 2000m, which has been taken as the depth of the water column (H) in the model used in this study.

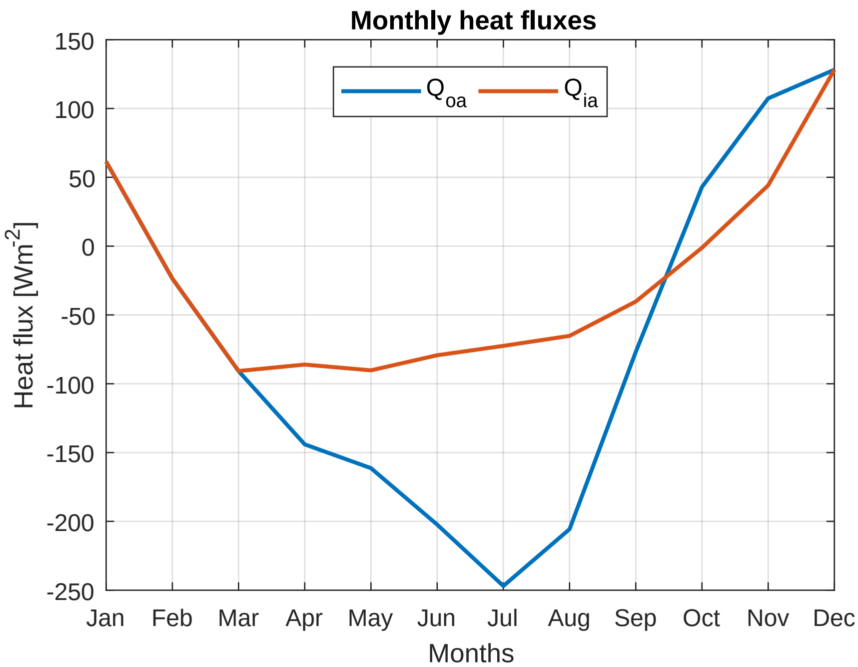

Fig. 16: The monthly heat fluxes in W m^{-2} determined from the CESM simulation of van Westen and Dijkstra (2019). The same data are displayed in Table 3. These values are interpolated linearly in the model as displayed in this figure. The data is determined using the method described in Section 3.1.

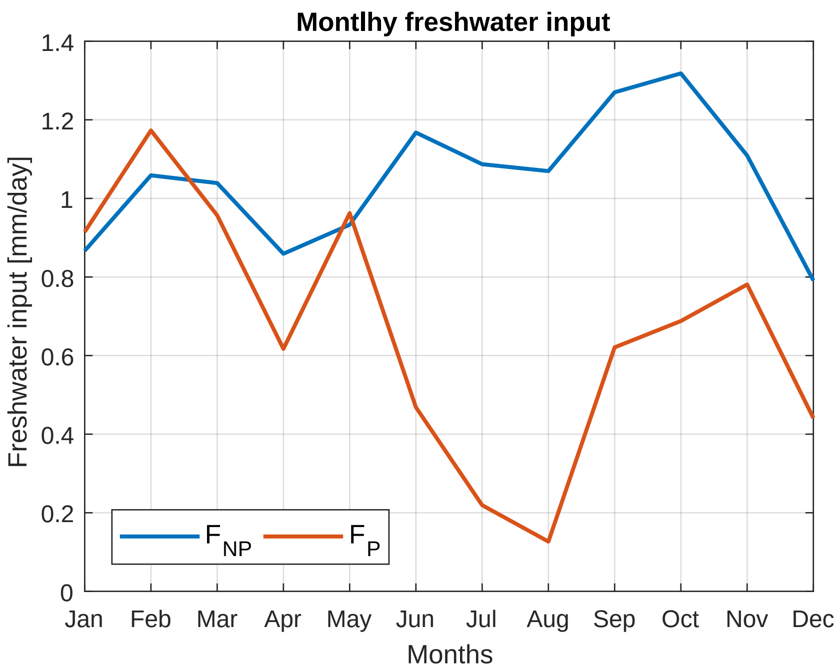

Fig. 17: The monthly freshwater input in mm/day determined from the CESM simulation of van Westen and Dijkstra (2019). The same data are displayed in Table 3. These values are interpolated linearly in the model as displayed in this figure. The data is determined using the method described in Section 3.1.